Mechanics of Materials 221 (2026) 105777

Contents lists available at ScienceDirect

Mechanics of Materials

journal homepage: www.elsevier.com/locate/mecmat

Research paper

Wrinkling analysis of a strain-limiting, implicit elastic membrane

Sandipan Paul

Department of Civil Engineering, Indian Institute of Technology Roorkee, Roorkee 247667, India

ARTICLE INFO

Invited Editor Ghatu Subhash

Keywords:
Wrinkles
Instability
Biological membranes
Implicit elasticity
Tension-field theory

ABSTRACT

In this paper, we investigate the wrinkling behavior of a strain-limiting membrane whose constitutive relations are derived from the theory of implicit elasticity. Specifically, a deformation mode-specific constitutive model, based on a set of scalar, conjugate stress/strain base pairs arising from a **QR** decomposition of the deformation gradient, has been considered for this analysis. A set of mixed strain and stress-based criteria have been used to distinguish between taut, wrinkled and slacked membranes. To determine the response of a wrinkled membrane, we impose a virtual deformation that stretches the membrane into a fictitious, taut state. The amount and direction of wrinkling are then obtained from the condition that the Cauchy stress, rotated into a local frame of reference of the wrinkled membrane, must be in a uniaxial, tensile state. This condition results in a system of two highly nonlinear, coupled, algebraic equations. In general, a closed-form analytical solution cannot be obtained for this system of equations and hence, a suitable numerical solution procedure must be adopted. Here we used a modified Broyden's method with a derivative-free line search algorithm to obtain a numerical solution to these equations and consequently, the response of the wrinkled membrane. Some relevant boundary value problems, corresponding to different displacement-controlled tests required for material characterization in the chosen framework, have been studied to show the efficacy of the developed model. Finally, we have discussed the effect of wrinkling on the identification of material parameters, along with analysis of wrinkling in anisotropic membranes.

1. Introduction

Biological tissues often exhibit a strain-limiting constitutive behavior in which the final stiffness is much higher than the initial one. Such a material behavior is commonly captured by introducing phenomenological models such as the ones proposed by Fung and coworkers (Fung, 1967; Tong and Fung, 1976; Fung, 2013). However, Freed and Rajagopal (2016a) showed that Fung's phenomenological model cannot be derived from a Helmholtz free energy for biological fibers. In fact, a thermodynamically consistent model to capture strain-limiting behavior is difficult to develop within the purview of a Green or Cauchy elasticity in which the stress is written as an explicit function of the corresponding measure of deformation. An effective way to circumvent this problem is to use a theory of implicit elasticity, proposed by Morgan (1966) and significantly developed by Rajagopal (2003). In this theory, it is argued that if the definition of an elastic body is extended to any continuum that is incapable of dissipation during a thermodynamic process, then it is possible to write the internal energy as a function of both stress and strain. This modified definition covers a broader class of elastic materials beyond the traditional Cauchy or Green elasticity. If $\mathbf{T}$ and $\mathbf{B}$ denote the Cauchy stress and the Finger tensor respectively, then the constitutive relation for these materials can be written in an implicit form as

$$\mathcal{G}(\mathbf{T}, \mathbf{B}) = 0. \tag{1}$$

It has been shown that this class of elastic bodies is capable of capturing a strain-limiting behavior without appealing to phenomenological models (Bulíček et al., 2015; Ortiz-Bernardin et al., 2014; Bustamante and Rajagopal, 2015). Based on this theory, Freed and Rajagopal (2016a) proposed a new model for biological fibers combining the response of its constituent collagen and elastin fibers. The collagen fibers account for the toe region of the experimentally observed stress–strain curve and their response is derived from a suitably chosen Gibbs free energy whereas the strain-limiting behavior, resulting from the response of the elastin fibers, is modeled using an implicit constitutive relationship of type (1). Later, this study was extended to account for the viscoelastic response of the collagen fibers (Freed and Rajagopal, 2016b) as well as a constitutive model for biological membranes (Freed et al., 2016). The latter model is of particular interest to our present study.

In general, the deformation of an elastic membrane is analyzed using a polar decomposition of the deformation gradient. However, in their model for biological membranes, Freed et al. (2016) used a different kinematic approach based on an upper-triangular (**QR**)

E-mail address: sandipan.paul@ce.iitr.ac.in.

https://doi.org/10.1016/j.mechmat.2026.105777
Received 13 April 2026; Received in revised form 27 May 2026; Accepted 20 June 2026
Available online 25 June 2026

decomposition of the deformation gradient (Srinivasa, 2012). Due to its practical utility in material characterization and ease of use, the **QR** kinematics has garnered considerable attention in the recent years and has been successfully employed in different areas of mechanics such as isotropic and anisotropic elasticity (Rajagopal, 2014; Srinivasa, 2015; Rajagopal and Srinivasa, 2016), plasticity (Paul and Freed, 2020, 2021; Paul, 2025), viscoelasticity and damage (J. Clayton and A. Freed, 2020), rheometry (Paul et al., 2021; Paudel and Paul, 2023), phase-field modeling of fracture (Hakimzadeh et al., 2022, 2025), and biomechanics (Avazmohammadi et al., 2018; Zhang et al., 2019; Kazerooni et al., 2019; J.D. Clayton and A. Freed, 2020; Zamani et al., 2021). Based on this kinematic framework, Freed (2017) showed that it is possible to develop constitutive models using appropriately defined scalar, conjugate, stress/strain base pairs that represent different modes of deformation. These conjugate stress/strain base pairs are particularly useful in the interpretation of experimental data as well as reducing computational cost in numerical simulations. For their analysis of biological membranes, Freed et al. (2016) used a 2-D version of their generalized model. They proposed a specific form of the internal energy as a function of both stress and strain attributes corresponding to three independent modes of deformation: a dilation, squeeze and shear. Although this model was able to capture the desired strain-limiting behavior, it ignores a key aspect of biological membranes for the sake of simplicity. Thin membranes are often considered to have negligible bending stiffness which causes it to deform only in tension. In the presence of compressive stresses along any of its principal stretch direction, a membrane either wrinkles or slacks. Although Freed et al. (2016) mentioned in passing that the wrinkling behavior can be analyzed using a tension field theory, they chose to ignore such cases in order to perform a simple planar analysis. Under this assumption, however, a wrinkle formation would have led to compressive stresses and strains that the membrane could not support. Therefore, this possibility was artificially suppressed by adding a Macaulay bracket in the stress–strain relationship corresponding to dilation. Although this model was able to capture the constitutive behavior of biological membranes, the artificial adjustment lacks proper physical justifications and does not elucidate the constitutive behavior of the membrane when wrinkling occurs. The aim of this paper is to address this missing aspect of their model of biological membranes. Specifically, we address two important concerns: *(i)* is non-negativity of the dilation stress a necessary and sufficient condition to prevent wrinkling? and, *(ii)* how does the stress–strain relationship change when the membrane wrinkles?

To incorporate wrinkling in a membrane model, a popular approach is the use of a tension-field theory (A. Pipkin, 1986; Steigmann and Pipkin, 1989a; Steigmann, 1990) in which a constitutive restriction is imposed by using a *relaxed strain energy* in the wrinkled region. A.C. Pipkin (1986) and Pipkin (1994) showed that the relaxed strain energy can be obtained through a *quasiconvexification* of the original strain energy used in the derivation of the constitutive relations for the taut membrane. Therefore, according to this theory, the strain energy for a membrane can be viewed as a composite function that has different expressions depending on whether the criteria for a taut, wrinkled or slacked membrane is satisfied. This method has been successfully employed to elastic, isotropic membranes of different geometry such as cylindrical (Peek, 2000; Patil et al., 2015) and toroidal membranes (Li and Steigmann, 1995; Roychowdhury and DasGupta, 2015), twisted ribbons (Kohn and O'Brien, 2018) as well as membranes with different material symmetry groups/properties such as fiber-reinforced (Shmoylova and Dorfmann, 2009) and orthotropic (Jarasjarungkiat et al., 2008) elastic membranes, viscoelastic membranes (Jenkins and Leonard, 1993; Weinberg and Neff, 2008) and Fung-type biological membranes (Massabò and Gambarotta, 2007) etc. The primary challenge of this approach, as stated by A.C. Pipkin (1986), is that there is no general procedure for the said quasiconvexification of the strain energy. For the implicit elastic model considered here, this process becomes even more convoluted since the internal energy is a function of both stress and strain. Therefore, we adopt here an alternative approach, proposed by Roddeman (1991), in which a virtual deformation is imposed on the wrinkled membrane such that it is stretched to a fictitious, taut state. Thereafter, the amount and direction of wrinkling are obtained from the condition that the Cauchy stress, rotated in the wrinkle frame of reference, is in a uniaxial, tensile state of stress, i.e., there exists exactly one positive, non-zero (normal) component of the rotated Cauchy stress. This condition essentially satisfies the requirement of a tension-field theory. Miyazaki (2006) showed that many of the existing wrinkle models for anisotropic membranes (Kang and Im, 1997; Epstein, 1999; Epstein and Forcinito, 2001) are essentially equivalent to this model. In most of the wrinkle models based on Roddeman (1991)'s approach such as Lu et al. (2001) and Jarasjarungkiat et al. (2008), an explicit stress–strain relationship was used that allowed for a direct numerical solution without resorting to an iterative procedure. For an implicit elastic membrane, however, this approach leads to a system of two highly nonlinear, coupled, algebraic equations that requires an iterative numerical method to determine the amount and direction of wrinkling at each time step. For this purpose, we use a modified Broyden's method (Broyden, 1965) with a derivative-free line search algorithm, proposed by Li and Fukushima (2000). Needless to say that once the amount and direction of wrinkling are obtained, the response of the wrinkled membrane can be derived by using the modified deformation gradient. The analysis of wrinkling carried out here shows that although the non-negativity of a dilational stress is a necessary condition for a taut, isotropic membrane as mentioned by Freed et al. (2016), this condition alone is not sufficient to ensure that the membrane under consideration is taut. In addition to having a positive value, the magnitude of the dilation stress must be greater than a certain numerical value that depends on both the squeeze and (scaled) shear stress attributes. In fact, the former condition does not hold true for an anisotropic membrane and is replaced by an inequality involving the dilation and squeeze stress attributes as well as the strength of anisotropy. As for the latter condition, it has an important consequence for an unequal-biaxial stretch of a strain-limiting membrane as shown in Section 4.2. It has been further observed that the stress–strain relationship for a wrinkled membrane differs significantly from that of a taut membrane which has an important implication on the identification of material parameters as discussed in Section 5.

The rest of the paper is organized as follows. In Section 2, we review the necessary kinematics and the constitutive relations for an implicit elastic membrane. For this section, our discussion is restricted to an assumption that the membrane remains taut throughout the motion. In Section 3, we derive the necessary and sufficient conditions to distinguish between a taut, wrinkled and slacked membrane. Thereafter, a numerical analysis to obtain the amount and direction of wrinkling is carried out. For this purpose, we adopt an iterative numerical solution strategy which has been derived in Section 3.3. In Section 4, some relevant boundary value problems have been studied to show the efficacy of the developed solution procedure. Specifically, we consider the problem of a simple shear, unequal-biaxial and uniaxial stretch (squeeze). In Section 5, the implications of wrinkling on the material characterization and the required modification in the solution strategy for an anisotropic membrane are discussed. Finally, the paper is summarized and drawn to conclusion. Although the findings in this paper show that the consideration of wrinkling significantly alters the experimental measurement of material parameters, our model prediction for the direction and amount of wrinkling is yet to be verified with the necessary experimental observations due to the current unavailability of suitable data. Therefore, the scope of the present work is limited to the development of a rigorous semi-analytical framework for biological membranes and a possible remedy for errors in their experimental characterization.

2. Preliminaries

2.1. Kinematics

Let us consider a thin, elastic, isotropic membrane $\mathcal{S}$ under a state of plane stress whose kinematics can be described by its mid-surface deformation. At time $t = 0$, the membrane is embedded into a two-dimensional Euclidean point space and occupies its undeformed configuration, $\kappa_R(\mathcal{S})$. $\mathbf{X}$ denotes the position vector of a material particle in $\kappa_R(\mathcal{S})$. Let $\mathbf{E}_\alpha, \alpha = 1, 2$ be two Cartesian base vectors that span the undeformed configuration of the membrane, $\kappa_R(\mathcal{S})$ and $\mathbf{E}_3$ is the normal to that plane such that $\mathbf{E}_3 = \mathbf{E}_1 \times \mathbf{E}_2$. A motion $\mathbf{x} = \mathcal{X}(\mathbf{X}, t)$ maps a material particle to its corresponding position $\mathbf{x}$ in the current configuration of the membrane, $\kappa_t(\mathcal{S})$. Hence, the deformation gradient $\mathbf{F}$ can be written as

$$\mathbf{F} = F_{i\alpha}\, \mathbf{e}_i \otimes \mathbf{E}_\alpha \quad \text{with} \quad F_{i\alpha} = \partial x_i / \partial X_\alpha \tag{2}$$

where $\mathbf{e}_i, i = 1, 2, 3$ are the base vectors spanning the current configuration of the membrane, $\kappa_t(\mathcal{S})$. From Eq. (2), one can notice that the matrix of the deformation gradient is a 3×2 matrix and takes into account the out-of-plane deformation of the membrane in a wrinkled or slacked state. In general, the deformed configuration of the membrane in these states cannot be defined *a priori*. Therefore, following Lu et al. (2001), we consider a smoothed pseudo-surface on which the material particles from the original deformed configuration of the membrane is projected. Hence, this pseudo-surface represents the deformed configuration of the membrane in an average sense. If $\tilde{\mathbf{e}}_\alpha, \alpha = 1, 2$ are two linearly independent base vectors that span the pseudo-surface, then the position vector of a material particle on this pseudo-surface can be represented as $\tilde{\mathbf{x}} = \tilde{x}_\alpha\, \tilde{\mathbf{e}}_\alpha$ and the corresponding (projected) deformation gradient $\tilde{\mathbf{F}}$ can be written as

$$\tilde{\mathbf{F}} = \tilde{F}_{\alpha\beta}\, \tilde{\mathbf{e}}_\alpha \otimes \mathbf{E}_\beta \quad \text{where} \quad \tilde{F}_{\alpha\beta} = \partial \tilde{x}_\alpha / \partial X_\beta, \quad \alpha, \beta = 1, 2. \tag{3}$$

Here as opposed to a polar decomposition, we adopt a **QR** decomposition of the deformation gradient, $\tilde{\mathbf{F}} = \mathcal{R}\,\mathcal{U}$ which results in an upper-triangular stretch tensor $\mathcal{U}$, called the Laplace stretch. The components of the Laplace stretch can be obtained either by performing a Gram–Schmidt procedure on the matrix of the projected deformation gradient $\tilde{\mathbf{F}}$ or through a Cholesky decomposition of the right Cauchy–Green tensor $\mathbf{C} \coloneqq \tilde{\mathbf{F}}^\top \tilde{\mathbf{F}} = \mathbf{F}^\top \mathbf{F} = C_{\alpha\beta}\, \mathbf{E}^\alpha \otimes \mathbf{E}^\beta$. Thus, the components of the Laplace stretch can be written as (Srinivasa, 2012)

$$[\mathcal{U}^\alpha_\beta] = \begin{bmatrix} a & a\,\gamma \\ 0 & b \end{bmatrix} = \begin{bmatrix} \sqrt{C_{11}} & C_{12}/\sqrt{C_{11}} \\ 0 & \sqrt{C_{22} - C_{12}^2/C_{11}} \end{bmatrix}$$

with

$$\begin{aligned} C_{11} &= \tilde{F}_{11}^2 + \tilde{F}_{21}^2 = F_{11}^2 + F_{21}^2 + F_{31}^2, \\ C_{12} &= \tilde{F}_{11}\tilde{F}_{12} + \tilde{F}_{21}\tilde{F}_{22} = F_{11}F_{12} + F_{21}F_{22} + F_{31}F_{32} \text{ and,} \\ C_{22} &= \tilde{F}_{12}^2 + \tilde{F}_{22}^2 = F_{12}^2 + F_{22}^2 + F_{32}^2. \end{aligned} \tag{4}$$

In this framework, the tensor $\mathcal{R}$ rotates a set of Eulerian base vectors $\tilde{\mathbf{e}}_\alpha$ into the base vectors $\mathcal{E}_\alpha$ that span a physical frame of reference in which the deformation gradient takes the form of an upper-triangular matrix. Thus, while the rotation tensor $\mathcal{R}$ takes part in coordinate transformation, the deformation of a material particle is completely specified by the Laplace stretch, $\mathcal{U}$. Let us further decompose the Laplace stretch into three modes of deformation as

$$[\mathcal{U}^\alpha_\beta] = \begin{bmatrix} a & a\,\gamma \\ 0 & b \end{bmatrix} = \underbrace{\sqrt{ab}\begin{bmatrix} 1 & 0 \\ 0 & 1 \end{bmatrix}}_{\text{Dilation}} \underbrace{\begin{bmatrix} \sqrt{a/b} & 0 \\ 0 & \sqrt{b/a} \end{bmatrix}}_{\text{Squeeze}} \underbrace{\begin{bmatrix} 1 & \gamma \\ 0 & 1 \end{bmatrix}}_{\text{Shear}} \tag{5}$$

Based on the decomposition in Eq. (5), we shall define the scalar, conjugate, stress/strain base pairs that will be used in our constitutive model.

Table 1
Strain, strain rate and stress attributes corresponding to different modes of deformation.

Deformation mode	Strain attributes	Strain rates	Stress attributes
Dilation	$\delta = 1/2\ln(ab)$	$\dot{\delta} = 1/2\left(\dot{a}/a + \dot{b}/b\right)$	$\pi = \mathcal{S}_{11} + \mathcal{S}_{22}$
Squeeze	$\varepsilon = 1/2\ln(a/b)$	$\dot{\varepsilon}_1 = 1/2\left(\dot{a}/a - \dot{b}/b\right)$	$\sigma = \mathcal{S}_{11} - \mathcal{S}_{22}$
Shear	γ	$\dot{\gamma}$	$\tau = a\,\mathcal{S}_{12}/b$

It is worth noting that, for a wrinkling analysis, the deformation gradient is often written in terms of the principal stretches using a polar decomposition of the deformation gradient as (Steigmann and Pipkin, 1989a,b)

$$\mathbf{F} = \zeta_1\, \mathbf{v_1} \otimes \mathbf{u_1} + \zeta_2\, \mathbf{v_2} \otimes \mathbf{u_2}. \tag{6}$$

Here ζ_1 and ζ_2 are the principal stretches, i.e., the eigenvalues of the stretch tensor $\mathbf{U}$ and, $\mathbf{v}_\alpha$ and $\mathbf{u}_\alpha$ are the eigenvectors of the stretch tensors $\mathbf{V}$ and $\mathbf{U}$ respectively. Since the eigenvectors are related through $\mathbf{v}_\alpha = \mathbf{R}\,\mathbf{u}_\alpha$, one can alternatively write

$$\mathbf{F} = \zeta_1\,(\mathbf{R}\mathbf{u_1}) \otimes \mathbf{u_1} + \zeta_2\,(\mathbf{R}\mathbf{u_2}) \otimes \mathbf{u_2} = \zeta_1\, \mathbf{v_1} \otimes (\mathbf{R}^\top \mathbf{v_1}) + \zeta_2\, \mathbf{v_2} \otimes (\mathbf{R}^\top \mathbf{v_2}). \tag{7}$$

One can notice a semblance of Eq. (7) with the expression of the Laplace stretch. In the **QR** kinematics framework, the Laplace stretch can be expressed as $\mathcal{U} = \mathcal{U}_{\alpha\beta}\, \mathcal{E}_\alpha \otimes \mathbf{E}_\beta$ where the base vectors $\mathcal{E}_\alpha$ of the physical frame of reference are related to that of the Eulerian frame through $\mathcal{E}_\alpha = \tilde{e}_\beta\, \mathcal{R}_{\alpha\beta}$. Therefore, while the matrix of the deformation gradient becomes a diagonal matrix when expressed in a rotated (through $\mathbf{R}$) frame of reference in which the eigenvectors of $\mathbf{U}$ and $\mathbf{V}$ serve as the base vectors, the Laplace stretch takes on the form of an upper triangular matrix in the physical frame of reference. As shown by Srinivasa (2012), the latter does not require a complex eigenvalue analysis and provides a direct path for the interpretation of experimental data (cf. Criscione et al., 2000; Criscione, 2003; Paul, 2025 for a detailed discussion). Thus, this framework helps in both numerical analysis as well as the experimental characterization of material parameters. The diagonal elements of the Laplace stretch, a and b represent an elongation along the $\mathcal{E}_\alpha$ direction whereas γ in the off-diagonal term represents the magnitude of shear. While the principal stretches ζ_1 and ζ_2 are important for the wrinkling analysis when a polar decomposition is used, the components of the Laplace stretch a, b and γ play a similar role in **QR** kinematics.

2.2. Constitutive model

To develop the required constitutive model, we first need to define a set of thermodynamic stress/strain conjugates that produce the mechanical stress power, $\dot{W}$. For this purpose, the Kirchhoff stress $J\,\mathbf{T}$ is pulled back into our physical frame of reference through $\mathcal{S} = \mathcal{R}^\top (J\,\mathbf{T})\,\mathcal{R}$. Now following Freed et al. (2016) and Freed (2017), we define the scalar conjugate stress/strain base pairs for the three modes of deformation as

Note that a similar choice for strains was also used by Lubarda (2010) in his analysis of biological membranes, albeit using a polar decomposition of the deformation gradient. In terms of these base pairs, the mechanical stress power can be written as

$$\dot{W} = \mathbf{S} : \dot{\mathbf{E}} = \mathcal{S} : \mathcal{L} = \pi\,\dot{\delta} + \sigma\,\dot{\varepsilon} + \tau\,\dot{\gamma} \tag{8}$$

where $\mathcal{L} \coloneqq \dot{\mathcal{U}}\,\mathcal{U}^{-1}$ is the velocity gradient associated with the Laplace stretch. Let us assume the existence of an internal energy density, ψ per unit reference area of the membrane. Following Rajagopal (2003), we further assume that the internal energy density is a function of both stress and strain attributes such that the rate of dissipation is zero. Thus, for an isothermal process, one can write

$$\mathrm{d}W = \rho_0 \mathrm{d}\psi \implies \pi\,\mathrm{d}\delta + \sigma\,\mathrm{d}\varepsilon + \tau\,\mathrm{d}\gamma$$

$$= \rho_0 \left(\frac{\partial \psi}{\partial \pi} \mathrm{d}\pi + \frac{\partial \psi}{\partial \delta} \mathrm{d}\delta + \frac{\partial \psi}{\partial \sigma} \mathrm{d}\sigma + \frac{\partial \psi}{\partial \varepsilon} \mathrm{d}\varepsilon + \frac{\partial \psi}{\partial \tau} \mathrm{d}\tau + \frac{\partial \psi}{\partial \gamma} \mathrm{d}\gamma \right) \tag{9}$$

where ρ_0 is the material density in the reference configuration. Since the modes of deformation are independent of each other, one can write the governing equations for each mode of deformation as

$$\left(\pi - \rho_0 \frac{\partial \psi}{\partial \delta} \right) \mathrm{d}\delta = \rho_0 \frac{\partial \psi}{\partial \pi} \mathrm{d}\pi \tag{10a}$$

$$\left(\sigma - \rho_0 \frac{\partial \psi}{\partial \varepsilon} \right) \mathrm{d}\varepsilon = \rho_0 \frac{\partial \psi}{\partial \sigma} \mathrm{d}\sigma \tag{10b}$$

$$\left(\tau - \rho_0 \frac{\partial \psi}{\partial \gamma} \right) \mathrm{d}\gamma = \rho_0 \frac{\partial \psi}{\partial \tau} \mathrm{d}\tau. \tag{10c}$$

Following Freed et al. (2016), we assume the specific form of the internal energy as

$$\rho_0\, \psi = 4\, A_1\, \delta - \pi + B_1\, \pi\, \delta + 2\, A_2\, \varepsilon - \sigma + B_2\, \sigma\, \varepsilon + A_3\, \gamma - \tau + B_3\, \tau\, \gamma \tag{11}$$

where A_i and $B_i, i = 1, 2, 3$ are the material parameters to be determined from experiments. While A_i represents the modulus for the corresponding mode of deformation, B_i denotes the reciprocal of the maximum strain attribute, i.e., $B_1 = 1/\delta_{\max}, B_2 = 1/\varepsilon_{\max}, B_3 = 1/\gamma_{\max}$ with $B_1\, \delta, B_2\, \varepsilon, B_3\, \gamma < 1$. Now using the assumed form for the internal energy in Eq. (11), Eqs. (10a)–(10c) can easily be integrated by separation of variables to determine the stress–strain relationship for each mode of deformation as

$$\pi = \frac{4 A_1\, \mathrm{sgn}(\delta)}{B_1 - 1} \left(\frac{1}{(1 - B_1 |\delta|)^{(1-1/B_1)}} - 1 \right), \tag{12a}$$

$$\sigma = \frac{2 A_2\, \mathrm{sgn}(\varepsilon)}{B_2 - 1} \left(\frac{1}{(1 - B_2 |\varepsilon|)^{(1-1/B_2)}} - 1 \right), \tag{12b}$$

$$\tau = \frac{A_3\, \mathrm{sgn}(\gamma)}{B_3 - 1} \left(\frac{1}{(1 - B_3 |\gamma|)^{(1-1/B_3)}} - 1 \right). \tag{12c}$$

Here 'sgn' denotes a signum function. The tangent moduli for different modes of deformation are obtained as

$$\frac{\partial \pi}{\partial \delta} = \frac{4 A_1 + (B_1 - 1)\pi}{1 - B_1 \delta}, \tag{13a}$$

$$\frac{\partial \sigma}{\partial \varepsilon} = \frac{4 A_2 + (B_2 - 1)\sigma}{1 - B_2 \varepsilon}, \tag{13b}$$

$$\frac{\partial \tau}{\partial \gamma} = \frac{4 A_3 + (B_3 - 1)\tau}{1 - B_3 \gamma}. \tag{13c}$$

Note that Freed et al. (2016) modeled a biological membrane by adding the contribution from elastin fibers, derived from a strain-limiting solid as well the contribution from collagen fibers that was considered to follow a simple Hookean law. In our discussion, we only consider the strain-limiting membrane for the sake of simplicity. We assume that the internal energy ψ is able to capture the overall stress–strain response of a biological membrane (i.e., collagen and elastin fibers together). A validation of this assumption is illustrated by comparing the resulting constitutive model (12) with the experimental data in Section 4. Furthermore, since the formation of wrinkles was not considered in their model, they adjusted the stress–strain relationship by using a Macaulay bracket on δ in Eq. (12a). This adjustment was carried out in order to suppress any possible compressive dilation stresses in the membrane. Although the constitutive model (12) was able to capture the experimental observations on taut biological membranes, the adjustment made to avoid wrinkling/slacking is essentially an artificial fix that lack proper physical justifications. Furthermore, this model does not address the changes in the constitutive behavior when the membrane is wrinkled. Thus, the following sections are devoted to address this missing aspect of the strain-limiting membrane model.

3. Wrinkling analysis

We now derive a suitable criteria to distinguish between a taut, wrinkled and slacked membrane and, determine the state of stresses and strains in the wrinkled region for the strain-limiting membrane described by the constitutive relation (12). For an isotropic Green elastic membrane, wrinkles form along the one of the principal directions[1] A. Pipkin (1986) and Steigmann (1990) and thus, computing *only* the amount of wrinkling is sufficient to obtain the full solution. However, the same is not true even for other material symmetry groups. Due to the complexity in the constitutive relations of an implicit elastic membrane considered here, it is expected that the wrinkle direction is also not known *a priori* in this case. Therefore, both the direction and amount of wrinkling need to be determined from suitable conditions.

3.1. Criteria for wrinkling

In the available literature, three types of criteria – a strain-based, stress-based and mixed criteria – have been used to determine the onset of wrinkling. A principal strain-based criteria classify the state of the membrane (i.e., taut, slacked or wrinkled) purely based on the eigenvalues of the relevant strain tensor such as a Green strain, $\mathbf{E}$ (Steigmann and Pipkin, 1989b; Massabò and Gambarotta, 2007). On the other hand, a stress-based criteria assess these states based on the magnitude and signs of the principal stresses (Epstein, 1999; Epstein and Forcinito, 2001). However, both these criteria misjudge the condition for at least one of the states of the membrane (Rossi et al., 2005; Jarasjarungkiat et al., 2008). Therefore, a mixed criterion based on both principal stresses and strains was proposed that proved to perform better in identifying these states. We adopt here this mixed criterion which is given as (Lu et al., 2001)

$$\begin{aligned}
&\text{taut:} && \mathbf{b}\cdot\mathbf{S}\mathbf{b} \geq 0 \implies \begin{cases} \mathrm{tr}(\mathbf{S}) = S_{11} + S_{22} \geq 0 \\ \det(\mathbf{S}) = S_{11} S_{22} - S_{12}^2 \geq 0 \end{cases} \\
&\text{slacked:} && \mathbf{a}\cdot\mathbf{E}\mathbf{a} \leq 0 \implies \begin{cases} \mathrm{tr}(\mathbf{E}) = E_{11} + E_{22} \leq 0 \\ \det(\mathbf{E}) = E_{11} E_{22} - E_{12}^2 \geq 0 \end{cases} \\
&\text{wrinkled:} && \text{otherwise}
\end{aligned} \tag{14}$$

Here $\mathbf{a}$ and $\mathbf{b}$ are arbitrary non-zero tangent vectors at a point in the undeformed configuration of the membrane respectively. $\mathbf{S}$ and $\mathbf{E}$ are the second Piola–Kirchhoff stress and the Green strain tensor respectively. Since the second Piola–Kirchhoff stress is related to the Cauchy stress through $\mathbf{S} = J \mathbf{F}^{-1}\, \mathbf{T}\, \mathbf{F}^{-\top}$ and $\mathbf{a}$ is an arbitrary vector, the first of Eq. (14) can be written in terms of the Cauchy stress as

$$\mathbf{c}\cdot\mathbf{T}\mathbf{c} \geq 0 \implies \begin{cases} T_{11} + T_{22} \geq 0 \\ T_{11} T_{22} - T_{12}^2 \geq 0 \end{cases} \tag{15}$$

where $\mathbf{c} = \mathbf{F}^{-\top}\mathbf{a}$ is an arbitrary tangent vector in the current configuration of the membrane, $\kappa_t(S)$.

Since our constitutive model is written in terms of the conjugate stress/strain base pairs, we need to rewrite the wrinkling criteria accordingly. For this purpose, let us start with the relationship between the components of the Laplace stretch and the eigenvalues of the right Cauchy–Green tensor, given in Eq. (4). The eigenvalues of the right Cauchy–Green tensor, $\mathbf{C}$ can be written as

$$\zeta_{1,2}^2 = \frac{1}{2} \left[(a^2(1+\gamma^2) + b^2) \pm \sqrt{(a^2(1+\gamma^2) + b^2)^2 - 4a^2 b^2} \right]. \tag{16}$$

Note that only in the absence of shear γ, the principal stretches become $\zeta_\alpha = a, b$. Otherwise a and b are distinct from the principal stretches.

[1] The directions of principal stresses and strains coincide for an isotropic material. We simply call them principal directions here.

Using Eq. (16), the eigenvalues of the Green strain tensor can be written as

$$\zeta^E_{1,2} = \frac{1}{4}\left[(a^2(1+\gamma^2)+b^2) \pm \sqrt{(a^2(1+\gamma^2)+b^2)^2 - 4a^2b^2}\right] - \frac{1}{2}. \qquad (17)$$

Therefore, according to Eq. $(14)_2$, a membrane is in its slacked state, i.e., it is not stretched in any direction when

$$\begin{aligned} \operatorname{tr}(\mathbf{E}) = \zeta^E_1 + \zeta^E_2 \le 0 \quad &\Longrightarrow (a^2-1)+(b^2-1)+a^2\gamma^2 \le 0, \\ \det(\mathbf{E}) = \zeta^E_1 \zeta^E_2 \ge 0 \quad &\Longrightarrow (a^2-1)(b^2-1) - a^2\gamma^2 \ge 0. \end{aligned} \qquad (18)$$

We now show that the condition (18) for a slacked membrane reduces to $0 \le a, b \le 1$ for any arbitrary value of γ. Since $a^2\gamma^2$ is always non-negative, Eq. (18) implies that

$$(a^2-1)+(b^2-1) \le -a^2\gamma^2 \le 0 \quad \text{and,} \quad (a^2-1)(b^2-1) \ge a^2\gamma^2 \ge 0. \qquad (19)$$

It is evident that Eq. (19) is satisfied only when $0 \le a, b \le 1$ irrespective of the value of the shear strain γ and thus, this inequality serves as a necessary condition for slacking. Let us understand the physical meaning of this condition. In our physical frame of reference, $a, b \ge 0$ represents the elongation of a material line element along the directions $\mathcal{E}_1$ and $\mathcal{E}_2$, respectively. Thus, $a, b > 1$ (or < 1) represents an elongation (or contraction) of a material line element along their respective directions. Therefore, the condition $0 \le a, b \le 1$, in the absence of shear γ, physically signifies that the membrane contracts in both $\mathcal{E}_1$ and $\mathcal{E}_2$ directions representing a slacked membrane. Since $0 \le a, b \le 1$ is valid for any arbitrary value of γ and does not impose any restriction on the shear mode of deformation, this condition alone is not sufficient to ensure slacking of a membrane. To determine the restriction on the shear strain γ due to slacking, let us first assume that γ can take any arbitrary value. Now from Eq. (18), one can write

$$a^2\gamma^2 \le 2 - a^2 - b^2 \quad \text{and,} \quad a^2\gamma^2 \le (a^2-1)(b^2-1). \qquad (20)$$

Since $0 \le a, b \le 1$ for a slacked membrane, it can be easily shown that $(a^2-1)(b^2-1) \le 2 - a^2 - b^2$. Thus, the restriction (20) on γ reduces to the inequality $\gamma^2 \le (1 - 1/a^2)(b^2 - 1)$. Therefore, this inequality along with the restriction $0 \le a, b \le 1$ represent the necessary and sufficient conditions for slacking of a membrane in our framework. To understand the physical meaning of the upper bound of γ for slacking, let us consider an initially slacked membrane with $0 < a, b < 1$ and $\gamma = 0$. Now let us apply a simple shear motion, i.e., $\gamma > 0$, keeping a and b fixed. As the extent of shear $a\gamma$ increases, the membrane reaches a state of deformation in which it is under tension in one direction while remains stress-free in the other and hence, the membrane is no longer in a slacked state. Therefore, an upper bound is required to ensure slacking which is represented by the inequality $\gamma^2 \le (1 - 1/a^2)(b^2 - 1)$.

For a taut membrane, the stresses must be non-compressive at a point in the membrane, as shown in Eq. $(14)_1$ or alternatively, Eq. (15). The Kirchhoff stress $\mathcal{S}$ in our physical frame of reference is related to the Cauchy stress $\mathbf{T}$ through $\mathcal{S} = \mathcal{R}^\top (J\mathbf{T})\mathcal{R}$. Therefore, the condition for a taut membrane (15) can be written as

$$\mathbf{c}\cdot\mathbf{T}\mathbf{c} = \mathcal{R}\mathbf{c}\cdot\mathcal{S}(\mathcal{R}\mathbf{c}) \ge 0$$
$$\Longrightarrow \begin{cases} \operatorname{tr}(\mathcal{S}) \ge 0 \implies \pi \ge 0 \\ \det(\mathcal{S}) \ge 0 \implies \pi^2 - \sigma^2 - 4b^2\tau^2/a^2 \ge 0. \end{cases} \qquad (21)$$

We have used the fact that $\mathcal{R}\mathbf{c}$ is also an arbitrary tangent vector in the derivation of Eq. (21). The condition (21) states that not only the dilation stress π must be non-negative, but its magnitude also has to be greater than a certain value that depends on the squeeze stress, σ and the scaled shear stress, $2b\tau/a$ for a membrane to be taut. Physically, Eq. $(21)_2$ ensures that the effect of a squeeze or shear mode of deformation is commensurately compensated by the dilation in order for a membrane to be taut. Although these conditions were qualitatively identified by Freed et al. (2016), their work does not provide the required mathematical descriptions which are derived in this paper. Moreover, only the first condition, $\pi \ge 0$, was used in their membrane model. It will be shown later in Section 4 that $\pi \ge 0$ alone is not a sufficient condition to correctly identify the onset of wrinkling for a strain-limiting membrane under a certain class of boundary value problems such as an unequal-biaxial stretch. We also notice that the condition $\pi \ge 0$ is identically satisfied if Eq. $(21)_2$ is written in the form $\pi \ge \sqrt{\sigma^2 + 4b^2\tau^2/a^2}$ where only positive square-root of the left hand side is taken into consideration. Therefore, this inequality is a necessary and sufficient condition for a membrane to be taut in our framework. To understand the physical meaning of this condition, let us consider a pure squeeze deformation in which the deformation gradient is an upper-triangular matrix, i.e., $\mathcal{R} = \mathbf{I}$. Under this condition, the only non-zero stress attribute is the squeeze stress, σ and thus, the matrix of the Cauchy stress tensor becomes a diagonal matrix with elements σ and $-\sigma$ (cf. Eq. (33)). Due to the presence of a compressive Cauchy stress component, the membrane no longer remains taut. A similar observation can also be made when the membrane is subjected to only a simple shear motion. Therefore, for a membrane to be taut, the dilation stress must compensate for the effects of squeeze and shear modes of deformation such that no compressive stress is generated anywhere in the membrane. This condition is ensured by the inequality $(21)_2$.

To summarize, the criteria to determine the state of a membrane in our physical frame of reference reads

$$\begin{aligned} &\text{taut:} && \pi \ge \sqrt{\sigma^2 + 4b^2\tau^2/a^2} \\ &\text{slacked:} && 0 \le a, b \le 1 \text{ and, } \gamma^2 \le (1 - 1/a^2)(b^2 - 1) \\ &\text{wrinkled:} && \text{otherwise} \end{aligned} \qquad (22)$$

3.2. Direction and amount of wrinkling

To analyze the state of strain and stress in a wrinkled membrane, we adopt the procedure proposed by Roddeman (1991) as a foundational framework with important modifications specific to our formulation. Let us consider a membrane with continuously distributed fine wrinkles in its deformed configuration, $\kappa_t(S)$.[2] We assume that in an infinitesimal neighborhood $\Omega \subset \kappa_t(S)$ around a material point, the wrinkles are in the direction of a unit vector $\mathbf{w}$ and let $\mathbf{t}$ be another unit vector perpendicular to it. As mentioned earlier, due to the lack of bending stiffness, a membrane cannot support compressive stresses. For a material point located in the wrinkled region of a membrane, a uniaxial state of stress exists in which the principal stress along the direction of wrinkling $\mathbf{w}$ is zero whereas the principal stress along its perpendicular direction remains tensile. Since the constitutive model (12) may result in compressive stresses in the wrinkled/slacked region that cannot be supported by a membrane, we need to modify this model such that the state of stress remains either tensile or zero. To obtain the strains and stresses at a point in the wrinkled region, let us impose a virtual stretch of amount β on the wrinkled membrane $\Omega \subset \kappa_t(S)$ such that it is locally lengthened into a fictitious, taut state, as shown in Fig. 1. Since a uniaxial state of stress is maintained throughout the deformation process until the membrane is fully taut, this virtual stretch is essentially a rigid body motion under a constant uniaxial state of stress. When the wrinkles just vanish, the deformation gradient takes the form (Roddeman, 1991; Lu et al., 2001)

$$\bar{\mathbf{F}} = (\mathbf{I} + \beta\,\mathbf{w}\otimes\mathbf{w})\,\tilde{\mathbf{F}} \qquad (23)$$

where $\mathbf{I}$ is the identity tensor in $\mathbb{R}^2$ and $\beta > 0$ is the stretch ratio that also serves as a measure for the amount of wrinkling. Since the virtual stretch β removes fine wrinkles from an infinitesimal neighborhood around a material point in $\kappa_t(S)$, the pair β and $\mathbf{w}$ provide a local description of wrinkles at that point in an average or continuum sense.

[2] There is an interesting semblance between this assumption and the ones used in continuum theories of defects that lead to definitions of geometrically necessary dislocation (GND) density tensor (Bilby et al., 1955; Cermelli and Gurtin, 2001) in plasticity and crack density tensor (Kachanov, 1980; Valanis and Panoskaltsis, 2005; Shivam and Paul, 2026) in damage mechanics.

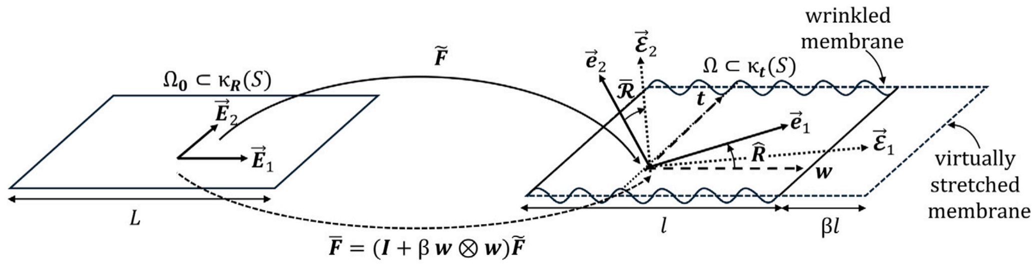

Fig. 1. A schematic diagram of the deformation of a membrane and the virtual stretching of the deformed membrane into a fictitious, taut state. The deformation gradient $\mathbf{F}$ and its modified form $\overline{\mathbf{F}}$ map the membrane from its undeformed configuration $\kappa_R(S)$ to its (wrinkled) deformed configuration $\kappa_t(S)$ and its corresponding fictitious taut configuration respectively. The latter configuration is obtained by a virtual stretching of the wrinkled membrane by an amount β along the direction $\mathbf{w}$.

Essentially, β and $\mathbf{w}$ can be viewed as spatially varying continuum fields and hence, this framework is valid for non-uniform wrinkle fields as well. It is important to note here that the framework is developed based on the assumption that wrinkling in a membrane occurs as a continuously distributed field of sufficiently fine wrinkles, which allows for a locally homogenized description of wrinkling at a material point. Such an assumption may not be valid for cases such as coarse wrinkling, occurrence of a few discrete wrinkles in the membrane or wrinkling dominated by boundary effects. Moreover, the exact information about a generated wrinkle such as wrinkle wavelength, amplitude and exact waviness profile also cannot be determined through this method. At present, however, we are interested in obtaining the deformation and response of the membrane in a continuum sense and the method of virtual stretch is well suited for this purpose.

For the deformation gradient in Eq. (23), the right Cauchy–Green tensor can be written as

$$\overline{\mathbf{C}} = \mathbf{C} + \beta(\beta+2)\,\overline{\mathbf{F}}^{\top}\mathbf{w} \otimes \overline{\mathbf{F}}^{\top}\mathbf{w}. \tag{24}$$

Let $\hat{\mathbf{T}}$ denote the Cauchy stress tensor in a new frame of reference with $\mathbf{w}$ and $\mathbf{t}$ as base vectors, referred to as the wrinkle frame of reference. This new coordinate frame $\{\mathbf{w}, \mathbf{t}\}$ is rotated out of the Eulerian frame of reference by an orthogonal tensor $\hat{\mathbf{R}} \in SO(2)$ and thus, the Cauchy stress in the Eulerian and wrinkle frame of reference are related through $\hat{\mathbf{T}} = \hat{\mathbf{R}}^{\top}\overline{\mathbf{T}}\hat{\mathbf{R}}$. Since the membrane is still in a uniaxial state in the $\{\mathbf{w}, \mathbf{t}\}$ frame of reference when the wrinkles just vanish, the modified Cauchy stress $\hat{\mathbf{T}}$ has only one non-zero component $\hat{\mathbf{T}}_{tt} > 0$. In other words, the modified Cauchy stress $\overline{\mathbf{T}}$ must satisfy the conditions

$$\mathbf{w} \cdot \overline{\mathbf{T}}\mathbf{w} = 0, \quad \mathbf{t} \cdot \overline{\mathbf{T}}\mathbf{w} = 0, \quad \mathbf{t} \cdot \overline{\mathbf{T}}\mathbf{t} > 0. \tag{25}$$

In terms of the Kirchhoff stress in our physical frame of reference, the condition (25) for a uniaxial state of stress can be written as

$$\hat{\mathbf{w}} \cdot \overline{\mathcal{S}}\,\hat{\mathbf{w}} = 0, \quad \hat{\mathbf{t}} \cdot \overline{\mathcal{S}}\,\hat{\mathbf{w}} = 0, \quad \hat{\mathbf{t}} \cdot \overline{\mathcal{S}}\,\hat{\mathbf{t}} > 0 \tag{26}$$

where $\hat{\mathbf{w}} = \overline{\mathcal{R}}^{\top}\mathbf{w}$ and $\hat{\mathbf{t}} = \overline{\mathcal{R}}^{\top}\mathbf{t}$ are the direction of wrinkling and its normal pulled back into our physical frame of reference. Note that a uniaxial state of stress in the principal directions is a fundamental requirement in the tension-field theory (A. Pipkin, 1986; Steigmann, 1990) as well. Here, the condition of a uniaxial state of stress is written in the wrinkle frame of reference instead of the principal directions.

The direction $\mathbf{w}$ and the measure of wrinkles β can be found by solving the system of highly nonlinear and coupled Eqs. $(25)_{1,2}$ or, $(26)_{1,2}$. Due to the high nonlinearity in our constitutive model (12), it is not possible to obtain a closed-form, analytical solution. In many of the earlier works on wrinkling analysis, e.g., Kang and Im (1997), Miyazaki (2006) and Jarasjarungkiat et al. (2008), a simple constitutive model such as $\mathbf{S} = \mathbb{C}\mathbf{E}$ was considered which greatly simplified the problem of solving the coupled Eqs. (25). However, the assumed St. Venant-Kirchhoff constitutive model is a direct extension of the generalized Hooke's law of linearized elasticity and is of extremely limited use in a finite deformation theory.

3.3. Numerical solution strategy

We now develop an appropriate numerical method to analyze an implicit, elastic membrane in a wrinkled state. Before solving the system of Eqs. (25), let us provide the relevant expressions that will be required in our numerical solution procedure. If the direction of wrinkling $\mathbf{w}$ makes an angle θ with the 1− co-ordinate direction of the Eulerian frame of reference $\mathbf{e}_1$, then $\mathbf{w}$ and $\mathbf{t}$ can be written in the form

$$\mathbf{w} = \begin{pmatrix} \cos\theta \\ \sin\theta \end{pmatrix} \quad \text{and,} \quad \mathbf{t} = \begin{pmatrix} -\sin\theta \\ \cos\theta \end{pmatrix} \quad \text{with the rotation matrix}$$
$$[\hat{R}_{ij}(\theta)] = \begin{bmatrix} \cos\theta & -\sin\theta \\ \sin\theta & \cos\theta \end{bmatrix}. \tag{27}$$

For a given value of the direction θ, measure of wrinkling β and deformation gradient $\mathbf{F}$, the modified Cauchy stress can be obtained via the following steps:

1. *Calculation of the Laplace stretch and rotation:* The matrix of the modified deformation gradient can now be written as

$$[\overline{F}_{ij}] = \begin{bmatrix} \bar{f}_1 & \bar{f}_2 \end{bmatrix}, \quad \text{with} \quad \bar{f}_1(\beta,\theta) = \begin{pmatrix} (1+\beta c^2)F_{11} + \beta c s F_{21} \\ \beta c s F_{11} + (1+\beta s^2)F_{21} \end{pmatrix},$$
$$\bar{f}_2(\beta,\theta) = \begin{pmatrix} (1+\beta c^2)F_{12} + \beta c s F_{22} \\ \beta c s F_{12} + (1+\beta s^2)F_{22} \end{pmatrix} \tag{28}$$

where $c \sim \cos\theta$, $s \sim \sin\theta$. In terms of the column vectors $\bar{f}_1$ and $\bar{f}_2$, the rotation matrix $\overline{\mathcal{R}}$ and the components of the Laplace stretch can be written as

$$[\overline{\mathcal{R}}_{ij}(\beta,\theta)] = \begin{bmatrix} \overline{\mathcal{E}}_1 & \overline{\mathcal{E}}_2 \end{bmatrix} \quad \text{with} \quad \overline{\mathcal{E}}_1 = \frac{\bar{f}_1}{\|\bar{f}_1\|},$$
$$\overline{\mathcal{E}}_2 = \frac{\bar{f}_2 - (\bar{f}_2 \cdot \bar{f}_1)\bar{f}_1}{\|\bar{f}_2 - (\bar{f}_2 \cdot \bar{f}_1)\bar{f}_1\|} \tag{29}$$

$$\bar{a} = \|\bar{f}_1\|, \quad \bar{\gamma} = \frac{\bar{f}_1 \cdot \bar{f}_2}{\|\bar{f}_1\|^2}, \quad \bar{b} = \sqrt{\|\bar{f}_2\|^2 - \frac{(\bar{f}_1 \cdot \bar{f}_2)^2}{\|\bar{f}_1\|^2}}. \tag{30}$$

Here a norm of a vector $\mathbf{a}$ is defined as $\|\mathbf{a}\| = \sqrt{\mathbf{a} \cdot \mathbf{a}}$.

2. *Calculation of the strain and stress attributes:* Now using the definition given in Table 1, the dilation and squeeze strain attributes are written as

$$\bar{\delta} = \frac{1}{2}\ln(\bar{a}\,\bar{b}) \quad \text{and,} \quad \bar{\varepsilon} = \frac{1}{2}\ln(\bar{a}/\bar{b}). \tag{31}$$

By using the constitutive model (12a)–(12c), the stress attributes are obtained as

$$\begin{aligned}\overline{\pi} &= \frac{4A_1\,\mathrm{sgn}(\overline{\delta})}{B_1-1}\left(\frac{1}{(1-B_1|\overline{\delta}|)^{(1-1/B_1)}}-1\right),\\ \overline{\sigma} &= \frac{2A_2\,\mathrm{sgn}(\overline{\varepsilon})}{B_2-1}\left(\frac{1}{(1-B_2|\overline{\varepsilon}|)^{(1-1/B_2)}}-1\right),\\ \overline{\tau} &= \frac{A_3\,\mathrm{sgn}(\overline{\gamma})}{B_3-1}\left(\frac{1}{(1-B_3|\overline{\gamma}|)^{(1-1/B_3)}}-1\right).\end{aligned} \tag{32}$$

3. *Determination of the modified Cauchy stress:* With these stress attributes, the modified Cauchy stress tensor in the Eulerian frame of reference can be written as

$$\overline{\mathbf{T}}(\beta,\theta)=\overline{\mathcal{R}}(\beta,\theta)\,\overline{\mathcal{S}}(\beta,\theta)\,\overline{\mathcal{R}}^{\top}(\beta,\theta)\quad\text{where}$$
$$[\overline{\mathcal{S}}_{ij}]=\begin{bmatrix}1/2(\overline{\pi}+\overline{\sigma}) & (\bar{b}/\bar{a})\overline{\tau}\\ (\bar{b}/\bar{a})\overline{\tau} & 1/2(\overline{\pi}-\overline{\sigma})\end{bmatrix}. \tag{33}$$

Now we are ready to determine the direction and amount of wrinkling by numerically solving Eqs. $(25)_{1,2}$. The main challenge to solve this problem is that our constitutive model (12) is highly nonlinear and formulated in a co-rotational frame of reference. Although the developed constitutive model is based on a rather simple set of *scalar* stress/strain base pairs, the various transformations required to connect the different frames of reference (viz., the Eulerian, physical and the wrinkle frame of reference) make the numerical analysis very difficult. In particular, an analytical computation of the Jacobian is nearly impossible for this system of equations. To avoid this issue, we adopt a modified Broyden's (Broyden, 1965) method along with a derivative-free line search algorithm, proposed by Li and Fukushima (2000). The problem can be reformulated within the numerical framework as: solve for $\mathbf{y}=(\beta \quad \theta)^{\top}$ with a prescribed deformation gradient $\mathbf{F}$[3] such that

$$\mathcal{F}(\mathbf{y})=\mathbf{0} \implies \begin{pmatrix}\hat{T}_{ww}(\mathbf{y})\\ \hat{T}_{wt}(\mathbf{y})\end{pmatrix}=\begin{pmatrix}\overline{T}_{11}(\mathbf{y})\,c^2+2\overline{T}_{12}(\mathbf{y})\,cs+\overline{T}_{22}(\mathbf{y})\,s^2\\ (\overline{T}_{11}(\mathbf{y})+\overline{T}_{22}(\mathbf{y}))\,cs-(c^2-s^2)\,\overline{T}_{12}(\mathbf{y})\end{pmatrix}$$
$$=\begin{pmatrix}0\\0\end{pmatrix}. \tag{34}$$

Eq. (34) can be solved by using the algorithm given by Zhou and Zhang (2020, Alg. 2.1) with an important modification for the update of the variables. For a strain-limiting membrane, the only admissible values for $\mathbf{y}=\left(\beta \quad \theta\right)^{\top}$ are those that generate a dilational, squeeze and shear strain that satisfy the conditions $B_1\,\delta, B_2\,\varepsilon$ and, $B_3\,\tau\le 1$. Therefore, a check for feasibility of the guessed values for $\mathbf{y}$ is required during the line search as well as the Broyden update steps within the algorithm. For the sake of completion, the modified algorithm is provided in Alg. 1. This algorithm requires five parameters, $p_1,p_2,p_3>0$ and, $q_1,q_2\in(0,1)$ as well as a positive sequence $\{\eta_k\}\Big|\sum_{k=0}^{\infty}\eta_k\le\eta<\infty$ to be suitably selected. The parameter q_3 is chosen such that $\left|q_{3_k}-1\right|\le q_3$ and the updated $\mathbf{B}_{k+1}$ is non-singular for any value of $q_3\in(0,1)$. For the current analysis, we have chosen $p_1=p_2=10^{-4}$, $p_3=0.9$, $q_1=0.5$, $q_2=0.9$, $q_3=1$ and $\eta_k=0.01/(k+1)^2$. Accuracy of the numerical procedure is susceptible to the chosen initial guess for θ. Therefore, the initial guess for θ should be judiciously chosen such that $\hat{\mathbf{T}}_{tt}$ remains positive throughout the motion. $\hat{\mathbf{T}}_{tt}>0$ ensures that the Cauchy stress, rotated into the wrinkle frame of reference, is in a uniaxial, *tensile* state.

4. Boundary value problems

In this section, we solve some boundary value problems with homogeneous deformations to show efficacy of the developed model.

[3] Typically in a FE analysis, an initial guess for the deformation gradient at the current time step is made and thereafter, its value is updated through an iterative scheme using the principal of virtual work. Hence, it is reasonable to assume that the (guessed) value of the deformation gradient is known at a particular iteration.

Table 2
Material parameters used in the numerical simulations.

	Dilation	Squeeze	Shear
Modulus (kPa)	$A_1=7$	$A_2=5$	$A_3=0.5$
1/Max. strain	$B_1=4$	$B_2=16$	$B_3=2$

Algorithm 1 A modified Broyden's method with Li-Fukushima line search algorithm for the numerical solution of Eq. (25)

Require: Initial point $\mathbf{y}_0\in\mathbb{R}^n$, non-singular $\mathbf{B}_0\in\mathbb{R}^{n\times n}$, Parameters $p_1,p_2,p_3>0$, $q_1,q_2\in(0,1)$
Require: A positive sequence $\{\eta_k\}\Big|\sum_{k=0}^{\infty}\eta_k\le\eta<\infty$, tolerance: tol >0
  $k\leftarrow 0$, $\mathcal{F}_k\leftarrow\mathcal{F}(\mathbf{y}_0)$
  while $\|\mathcal{F}_k\|>$ tol **do**
    Compute $\mathbf{d}_k^B=-\mathbf{B}_k^{-1}\mathcal{F}_k$
    $\mathbf{z}_k=\mathbf{y}_k+\mathbf{d}_k^B$
      Check: feasibility of $\mathbf{z}_k$
    if $\|\mathcal{F}(\mathbf{z}_k)\|>p_3\,\|\mathcal{F}_k\|$ **then**
      $\mathbf{d}_k\leftarrow\mathbf{d}_k^B$
    else
      Compute $\mathbf{d}_k^{MB}=-\mathbf{B}_k^{-1}\mathcal{F}(\mathbf{z}_k)$
      if $\left\|\mathcal{F}(\mathbf{y}_k+\mathbf{d}_k^B+\mathbf{d}_k^{MB})\right\|\le q_2\,\|\mathcal{F}_k\|-p_1\left\|\mathbf{d}_k^B+\mathbf{d}_k^{MB}\right\|^2$ **then**
        $\mathbf{d}_k\leftarrow\mathbf{d}_k^B+\mathbf{d}_k^{MB}$, $\alpha_k\leftarrow 1$
      else
        $\mathbf{d}_k\leftarrow\mathbf{d}_k^B$
      end if
    end if
      Check: feasibility of $\mathbf{y}_k+\mathbf{d}_k$
    if $\|\mathcal{F}(\mathbf{y}_k+\mathbf{d}_k)\|\le q_2\,\|\mathcal{F}_k\|-p_1\,\|\mathbf{d}_k\|^2$ **then**
      $\alpha_k\leftarrow 1$
    else
      $\alpha_k\leftarrow 1$
      while $\|\mathcal{F}(\mathbf{y}_k+\alpha_k\,\mathbf{d}_k)\|>\|\mathcal{F}_k\|-p_2\,\|\alpha_k\,\mathbf{d}_k\|^2+\eta_k\,\|\mathcal{F}_k\|$ **do**
        $\alpha_k\leftarrow q_1\,\alpha_k$
        Check: feasibility of $\mathbf{y}_k+\alpha_k\,\mathbf{d}_k$
      end while
    end if
    $\mathbf{y}_{k+1}\leftarrow\mathbf{y}_k+\alpha_k\,\mathbf{d}_k$
    $\mathbf{s}_k\leftarrow\mathbf{y}_{k+1}-\mathbf{y}_k$
    $\mathcal{G}_k\leftarrow\mathcal{F}(\mathbf{y}_{k+1})-\mathcal{F}_k$
    if $\|\mathbf{s}_k\|>0$ **then**
      $\mathbf{B}_{k+1}\leftarrow\mathbf{B}_k+q_3\,\dfrac{(\mathcal{G}_k-\mathbf{B}_k\,\mathbf{s}_k)\,\mathbf{s}_k^{\top}}{\|\mathbf{s}_k\|^2}$
    else
      $\mathbf{B}_{k+1}\leftarrow\mathbf{B}_k$
    end if
    $\mathcal{F}_{k+1}\leftarrow\mathcal{F}(\mathbf{y}_{k+1})$
    $k\leftarrow k+1$
  end while
    return $\mathbf{y}_k$

The chosen motions correspond to different displacement-controlled tests that are required for characterizing the material parameters of biological membranes. For the numerical simulations performed here, we have selected the material parameters used by Freed et al. (2016) which are obtained through an experimental verification with data from double-lap shear test on porcine myocardium (Dokos et al., 2002) and biaxial test on porcine visceral pleura (Freed et al., 2014). The material parameters are provided in Table 2 and, comparisons between the constitutive model (12) using these material parameters and the experimental data are shown in Fig. 2. It is worth noting here that some minor adjustments were made to the material parameters used by Freed

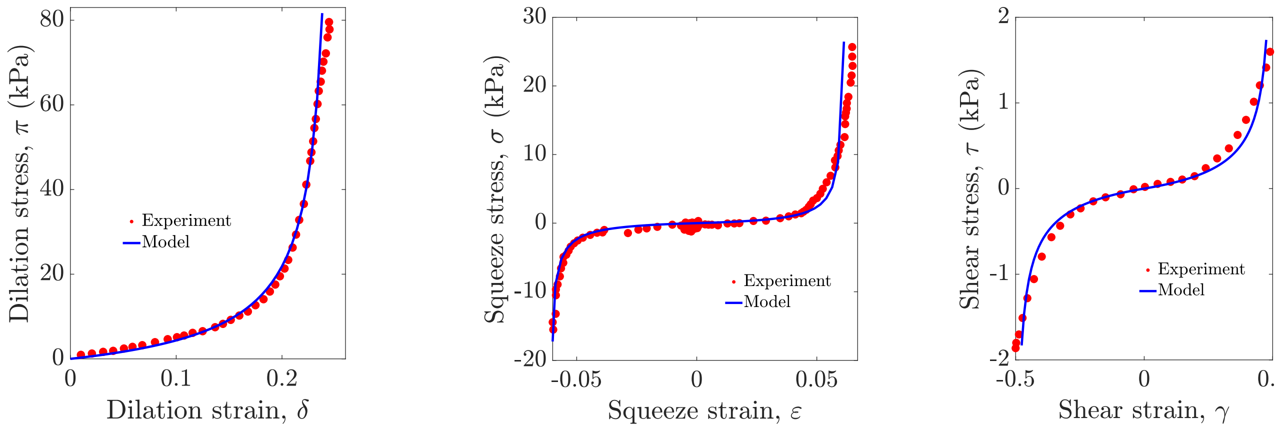

(a) (b) (c)

Fig. 2. Comparison of the constitutive model (12) with the experimental data of Freed et al. (2014) for the dilation and squeeze modes of deformation and Dokos et al. (2002) for a simple shear. The constitutive model shows a very good match with the experimental data.

et al. (2016) since we do not consider a linear, elastic contribution from the collagen fibers separately. The comparisons in Fig. 2 demonstrate that the constitutive model (12), which incorporates the contributions from both elastin and collagen fibers together, shows a very good match with the corresponding experimental data.

4.1. Simple shear

Let us consider a rectangular membrane of dimensions $L \times W$ along the laboratory axes $\mathbf{E}_1$ and $\mathbf{E}_2$, subjected to a motion

$$x_1 = X_1 + \xi(t)\, X_2, \quad x_2 = X_2, \quad \xi(t) \geq 0 \quad \text{with} \quad \xi(0) = 0. \tag{35}$$

This motion results in a deformation gradient of the form

$$[\tilde{F}_{\alpha\beta}] = \begin{bmatrix} 1 & \xi(t) \\ 0 & 1 \end{bmatrix}. \tag{36}$$

This deformation gradient corresponds to a motion applied in a simple shear test such as the double 4-bar shear experiments performed by Sridhar et al. (2025). In this experimental setup, they used three clamps — two transverse clamps that provide the essential displacement boundary conditions and a relatively thin clamp placed in the middle of the sample that moves by a linear actuator to produce the required simple shear. The deformation of the sample and the associated stresses are measured using a digital image correlation (DIC) technique and with the help of appropriately placed load cells, respectively. More details on the experimental test setup can be found in the original paper (Sridhar et al., 2025).

For this problem, we further assume that the membrane is subjected to a constant shear rate, i.e., $\dot{\xi}$ = a positive constant. Since the matrix of the deformation gradient is upper-triangular, the rotation $\mathcal{R}$ is an identity map and the matrix of the Laplace stretch is the same as that of the deformation gradient with $a = b = 1$ and $\gamma = \xi(t)$. From Eq. (36), it is evident that the shear strain γ is the only non-zero strain attribute for this motion. Thus, the strain attributes can be written as

$$\delta = \varepsilon = 0, \quad \gamma = \xi(t). \tag{37}$$

Let us assume that the membrane is initially taut. Under this condition, the stress attributes are obtained via the constitutive model (12) as

$$\pi = \sigma = 0, \quad \tau = \frac{A_3}{B_3 - 1}\left(\frac{1}{(1 - B_3\xi(t))^{(1-1/B_3)}} - 1\right). \tag{38}$$

Note that for the prescribed deformation gradient, $a = b = 1$ and $\gamma \geq 0$ at all stages of deformation which violates the condition $(22)_2$ for slacking. On the other hand, since $\gamma(t) > \pi = 0$, the condition for a taut membrane $(22)_1$ is also violated. Therefore, one can conclude that the membrane wrinkles as soon as the motion starts. Now we shall determine the wrinkle direction θ and the amount of wrinkling β at each time step using the method developed in Section 3.3.

Results of the numerical simulations to solve Eq. (34) are shown in Fig. 3. Fig. 3(a) shows the variation of the $\hat{T}_{ww}$ and $\hat{T}_{wt}$ components of the Cauchy stress rotated in the wrinkle frame of reference, $\{\mathbf{w}, \mathbf{t}\}$. Note that the residual $\mathcal{F}(\mathbf{y})$ in Eq. (34) comprises of these two components and hence, Fig. 3(a) represents the measures of error in the numerical solution. The maximum error for the numerical solution, computed as $\max\limits_{\forall \xi(t)} \sqrt{\hat{T}_{ww}^2 + \hat{T}_{wt}^2}$, is reported to be 9.92×10^{-9}. Fig. 3(b) shows the variation of the remaining component $\hat{T}_{tt}$ of the rotated Cauchy stress with the applied shear strain $\xi(t)$. As required, $\hat{T}_{tt}$ remains positive throughout the motion which implies that the Cauchy stress in the wrinkle frame of reference is under a uniaxial state of *tensile* stress. The variation of the amount and direction of wrinkles are shown in Figs. 3(c) and 3(d), respectively. Both the amount of wrinkling β and the value of θ increase as the motion proceeds.

Fig. 4 shows the variation of different stress attributes with the applied shear strain $\xi(t)$. It is interesting to note that although the maximum applied shear strain $\xi(t)$ is less than that prescribed in Table 2, i.e., $\max\{\xi(t)\} < 1/B_3 = 0.5$, a shear strain greater than $\xi(t) \simeq 0.23$ cannot be applied to the membrane. This is due to the fact that in the presence of wrinkles, the squeeze strain generated in the membrane exceeds its maximum value of $1/B_2 = 0.0625$ when $\xi(t) \simeq 0.23$. Fig. 4(b) shows the effect of wrinkling on the shear stress attribute τ as compared to the taut membrane (i.e., without the consideration of wrinkling) given in Eq. (38). It can be observed that the shear stress for the wrinkled membrane varies more gradually as compared to a taut membrane. The effects of wrinkling are more pronounced on the dilation and squeeze stress attributes. For a taut membrane, the stress attributes π and σ are both zero since $a = b = 1$ throughout the motion. However, this is not true in the presence of wrinkles as the deformation gradient is modified to account for wrinkling as per Eq. (23). The dilational stress is found to be significantly higher than the squeeze stress when wrinkling is taken into account.

4.2. Biaxial stretch

Let us now consider that the membrane is subjected to a motion

$$x_1 = (1 + \lambda(t))\, X_1, \quad x_2 = (1 + \nu\, \lambda(t))\, X_2,$$
$$\lambda(t) \geq 0 \quad \text{with} \quad \lambda(0) = 0, \quad 0 < \nu \leq 1. \tag{39}$$

This motion corresponds to a displacement-controlled biaxial test setup in which a sample is attached to four clamps on all sides of a suitably prepared sample. These clamps are then subjected to controlled

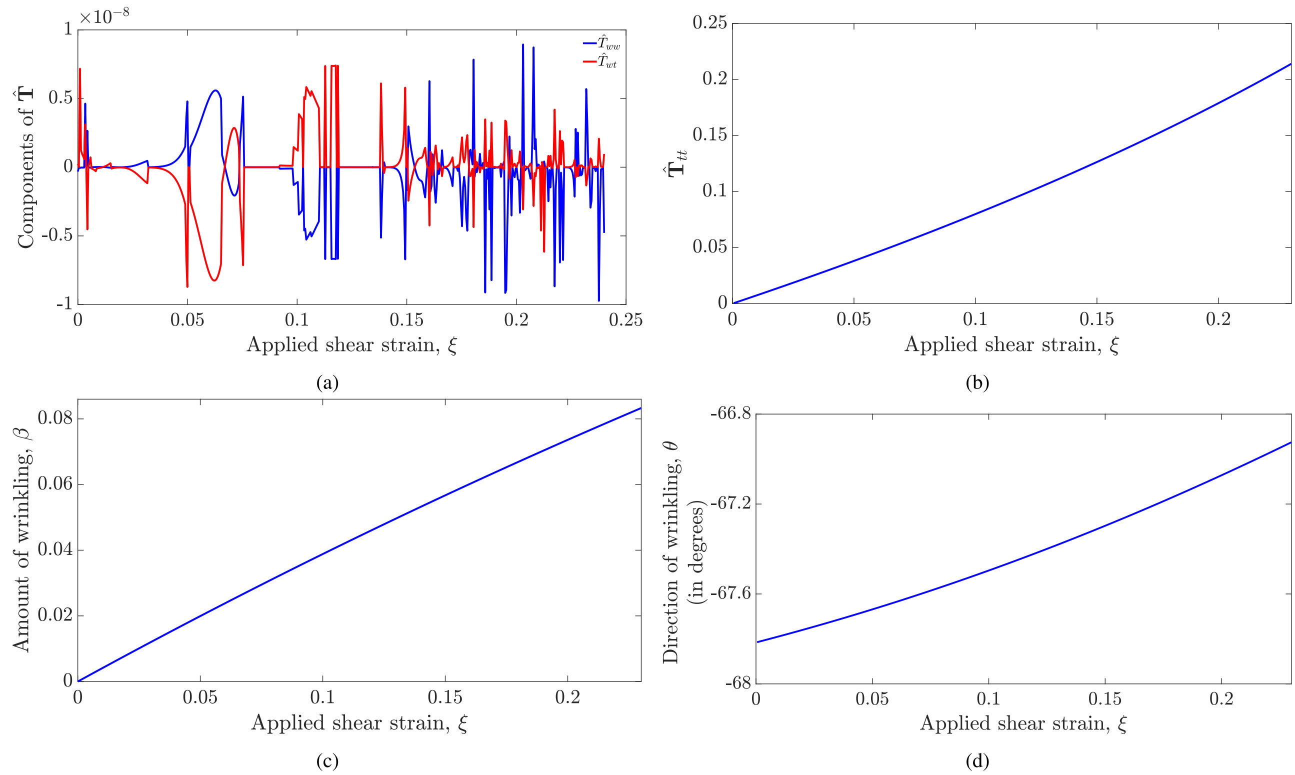

Fig. 3. Results of numerical analysis for wrinkling under a simple shear. Variation of: (a) the $\hat{T}_{ww}$ and $\hat{T}_{wt}$ components of the Cauchy stress rotated in the $\{\mathbf{w}, \mathbf{t}\}$ frame of reference that serve as a measure of errors in the analysis, (b) the rotated Cauchy stress component $\hat{T}_{tt}$ (c) the amount of wrinkling, β and (d) its direction, θ with the applied shear strain, $\xi(t)$.

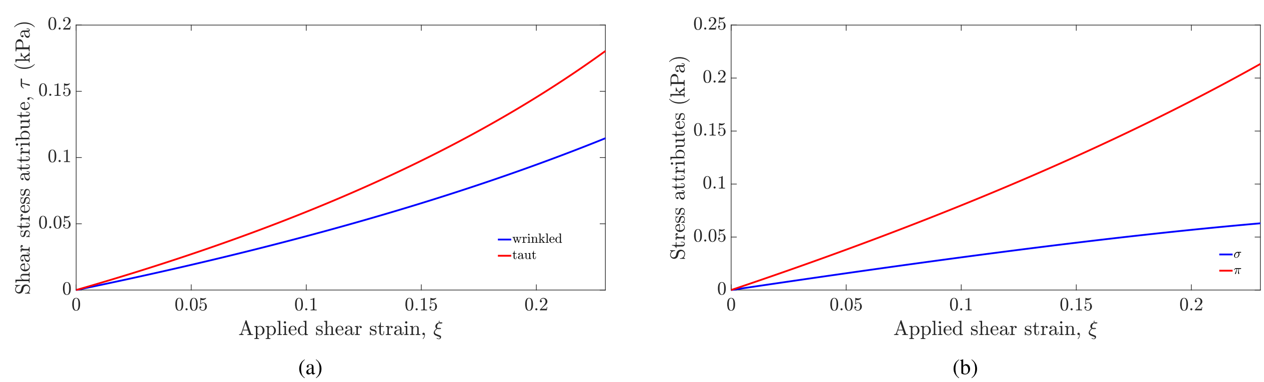

Fig. 4. Variation of : (a) the shear stress attribute, τ for a wrinkled and a taut (without the consideration of wrinkles) membrane and, (b) the squeeze stress attribute, σ and the dilation stress attribute, π with the applied shear strain $\xi(t)$.

displacements $\lambda(t)$ and $\nu\lambda(t)$ producing the required biaxial stretch condition. More details on the biaxial test setups can be found in Sacks and Sun (2003), Fehervary et al. (2016), Jiang et al. (2021) and the references therein. An equibiaxial stretch is a special case of this motion when $\nu = 1$. Let us further assume that $\dot{\lambda}(t) =$ a positive constant. For this motion, the matrices of the deformation gradient, rotation tensor and the Laplace stretch are written as

$$[\tilde{F}_{ij}] = [\mathcal{U}_{ij}] = \begin{bmatrix} 1+\lambda(t) & 0 \\ 0 & 1+\nu\lambda(t) \end{bmatrix}, \quad [\mathcal{R}_{ij}] = \begin{bmatrix} 1 & 0 \\ 0 & 1 \end{bmatrix}. \tag{40}$$

Therefore, the strain and stress attributes are obtained from Table 1 as

$$\delta = \frac{1}{2}\ln\left(1 + (1+\nu)\,\lambda + \nu\,\lambda^2\right), \quad \varepsilon = \frac{1}{2}\ln\left(\frac{1+\lambda}{1+\nu\,\lambda}\right), \quad \gamma = 0 \tag{41}$$

and,

$$\pi = \frac{4A_1}{B_1 - 1}\left(\frac{1}{(1-B_1\delta)^{(1-1/B_1)}} - 1\right),$$

$$\sigma = \frac{2A_2}{B_2 - 1}\left(\frac{1}{(1-B_2\varepsilon)^{(1-1/B_2)}} - 1\right), \quad \tau = 0. \tag{42}$$

From Eq. (40), it is evident that the membrane does not slack at any stage of the deformation since $a, b > 1$. For an equibiaxial stretch ($\nu = 1$), the squeeze strain and stress becomes zero, i.e., $\varepsilon = \sigma = 0$ and hence, the criterion for a taut membrane $(22)_2$ is always satisfied. In this case, the complete state of strain and stress are given by Eqs. (41) and (42) with a slight modification for the squeeze mode as $\varepsilon = \sigma = 0$. On the other hand, for an unequal-biaxial stretch, whether a membrane is taut or wrinkled depends on the specific values of π and σ. Specifically, the wrinkling criteria (22) reduces to

$$|\pi| \geq |\sigma| \rightarrow \text{taut}, \quad |\pi| < |\sigma| \rightarrow \text{wrinkled}. \tag{43}$$

Note that unlike the simple shear deformation in Section 4.1, the wrinkling criterion for an unequal-biaxial stretch depends on both the numerical values of λ and ν describing the motion as well as the

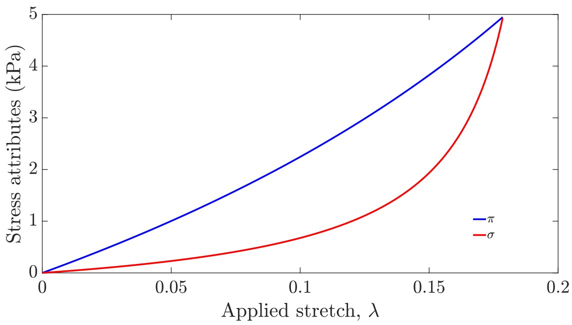

(a)

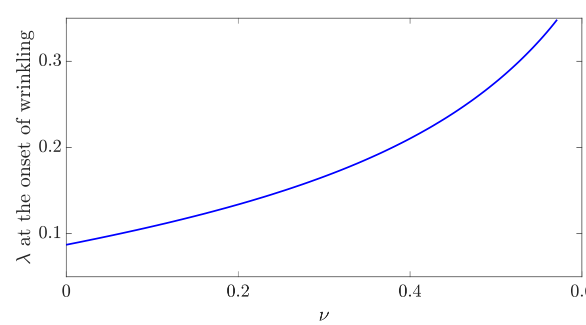

(b)

Fig. 5. (a) A typical variation of different stress attributes with the applied stretch $\lambda(t)$ for an unequal biaxial stretch with $\nu = 0.3$ when the membrane is taut. (b) Variation of the value of the applied stretch λ at the onset of wrinkling with ν.

material properties A_1, A_2, B_1 and B_2. Therefore, the wrinkling criterion also needs to be identified during the numerical solution. Fig. 5(a) shows a typical variation of the stress attributes with the applied stretch $\lambda(t)$ for a taut membrane undergoing unequal-biaxial stretch for $\nu = 0.3$. Throughout the deformation, the shear stress τ remains zero whereas the dilation and squeeze stresses increase with the applied stretch λ. Although over the chosen range of deformation, the magnitude of the dilation stress is greater than that of the squeeze stress ensuring a taut state of the membrane, this relationship reverses around $\lambda = 0.167$. This is due to the fact that the squeeze stress attribute, σ shows a sharp stiffening near $\lambda \simeq 0.167$ as the strain-limiting effect becomes significant in the squeeze mode of deformation. With further stretch beyond the range shown in Fig. 5(a), the magnitude of the squeeze stress exceeds that of the dilation stress causing the membrane to wrinkle. It is emphasized that this phenomena is unique to a strain-limiting elastic membrane in which the maximum dilation strain is greater than the maximum squeeze/shear strains. Fig. 5(b) shows the variation of the values of the applied stretch λ at the onset of wrinkling with ν. The value of λ at the onset of wrinkling increases with ν until $\nu \simeq 0.57$, after which the membrane remains taut for a wider range of $\lambda(t)$. Equibiaxial stretch is a limiting case of $\nu > 0.57$ in which the membrane remains taut throughout the motion. Note that the applied stretch required for wrinkling also depends on the material properties; Fig. 5(b) shows the variation of such values of the applied stretch, λ *only* for the material properties given in Table 2.

To show the behavior of a wrinkled membrane under an unequal-biaxial stretch, we performed numerical simulations for $\nu = 0.3$. Fig. 6 shows the results of this numerical analysis. As shown in Fig. 5, the membrane transitions from taut to wrinkled state at $\lambda \simeq 0.167$. Therefore, while Eqs. (12a)–(12c) are used for $\lambda \le 0.167$, the stress attributes for the membrane can be found by using the numerical procedure described in Section 3.3 for $\lambda > 0.167$. Figs. 6(a) and 6(b) show the variation of different components of the rotated Cauchy stress $\hat{\mathbf{T}}$. From the discussion in Section 3.3, it is evident that $\hat{T}_{ww}$ and $\hat{T}_{wt}$ serve as the measure of error in the numerical analysis of wrinkles. The maximum error for this analysis is found to be 9.39×10^{-9}. Moreover, as shown in Fig. 6(b), $\hat{T}_{tt}$ has an increasing positive value during the wrinkle analysis ensuring that $\hat{\mathbf{T}}$ is in a uniaxial, tensile state. As can be observed from Fig. 6(c), the amount of wrinkling, β increases linearly with the applied stretch λ as the deformation progresses. On the other hand, the direction of wrinkling remains constant at $\theta \simeq 90°$ as shown in Fig. 6(d), i.e., wrinkles form in a direction perpendicular to the applied stretch λ.

Variations of the dilational stress π and the squeeze stress σ over the admissible range of the applied stretch λ are shown in Fig. 7. As discussed earlier, the stress attributes are determined through the constitutive equations (12a) and (12b) up to a stretch of $\lambda = 0.167$ since the condition for a taut membrane is met over this range of λ. Thereafter, the membrane wrinkles as the squeeze stress exceeds the dilational stress due to the strain-limiting behavior in the squeeze mode of deformation and hence, the stress attributes are obtained via the numerical procedure, described in Section 3.3. For $\lambda > 0.167$, the dilational and squeeze stress attributes, obtained from the modified deformation gradient as per Eq. (23), coincide (i.e., $\bar{\sigma} = \bar{\pi}$), as shown in Fig. 7. Since the matrix of the deformation gradient is a diagonal matrix, it is evident that $\overline{\boldsymbol{\mathcal{R}}} \simeq \mathbf{I}$ and $\overline{\mathbf{T}} \simeq \overline{\boldsymbol{\mathcal{S}}}$. Thus in view of Eq. (33), $\bar{\sigma} = \bar{\pi}$ implies that $\bar{T}_{11} = \bar{\mathcal{S}}_{11} = \bar{\pi}$ and $\bar{T}_{22} = \bar{\mathcal{S}}_{22} = 0$. Now a rotation of the Cauchy stress by $\theta \simeq 90°$ ensures that a uniaxial state of stress exists for $\hat{\mathbf{T}}$ in which $\hat{T}_{ww} = \hat{T}_{wt} = 0$ and $\hat{T}_{tt} = \bar{\pi} > 0$. A similar pattern for the variation of the amount and direction of wrinkling as well as the stress attributes can be observed for other values of ν within the range $0 < \nu < 0.57$.

4.3. Uniaxial stretch

Let us consider an area-preserving uniaxial stretch (or squeeze along $\mathbf{E}_1$ and $\mathbf{E}_2$) of an initially undeformed membrane. A biaxial testing platform, such as the one developed by Jiang et al. (2021), is also able to produce this motion when a suitably prepared, nearly incompressible sample is attached to two clamps and stretched in a particular direction. The deformation map for this motion is given as

$$x_1 = \Lambda(t)\, X_1, \quad x_2 = \frac{1}{\Lambda(t)}\, X_2, \quad \Lambda(t) > 0 \quad \text{with} \quad \Lambda(0) = 1. \tag{44}$$

Let $\dot{\Lambda}(t)$ be a positive constant. For this motion, the deformation gradient, rotation tensor and the Laplace stretch are similar to Eq. (40) and are written as

$$[\tilde{F}_{ij}] = [\mathcal{U}_{ij}] = \begin{bmatrix} 1+\Lambda(t) & 0 \\ 0 & 1/(1+\Lambda(t)) \end{bmatrix}, \quad [\mathcal{R}_{ij}] = \begin{bmatrix} 1 & 0 \\ 0 & 1 \end{bmatrix}. \tag{45}$$

Note that in this case, $a > 1$ whereas $b < 1$ and hence, the membrane also does not slack. This is also true when $\dot{\Lambda}$ takes a negative value which results in $a < 1$ but $b > 1$. The strain and stress attributes for this deformation are given as

$$\delta = \gamma = 0, \quad \varepsilon = \ln(1 + \Lambda), \tag{46}$$

$$\pi = \tau = 0, \quad \sigma = \frac{2A_2}{B_2 - 1}\left(\frac{1}{(1 - B_2\varepsilon)^{(1-1/B_2)}} - 1\right). \tag{47}$$

Since $\sigma > \pi = 0$ throughout the motion, the membrane wrinkles as soon as the deformation starts, just like a membrane under simple shear. The state of stress and strain of the wrinkled membrane can be found by using the numerical method given in Section 3.3.

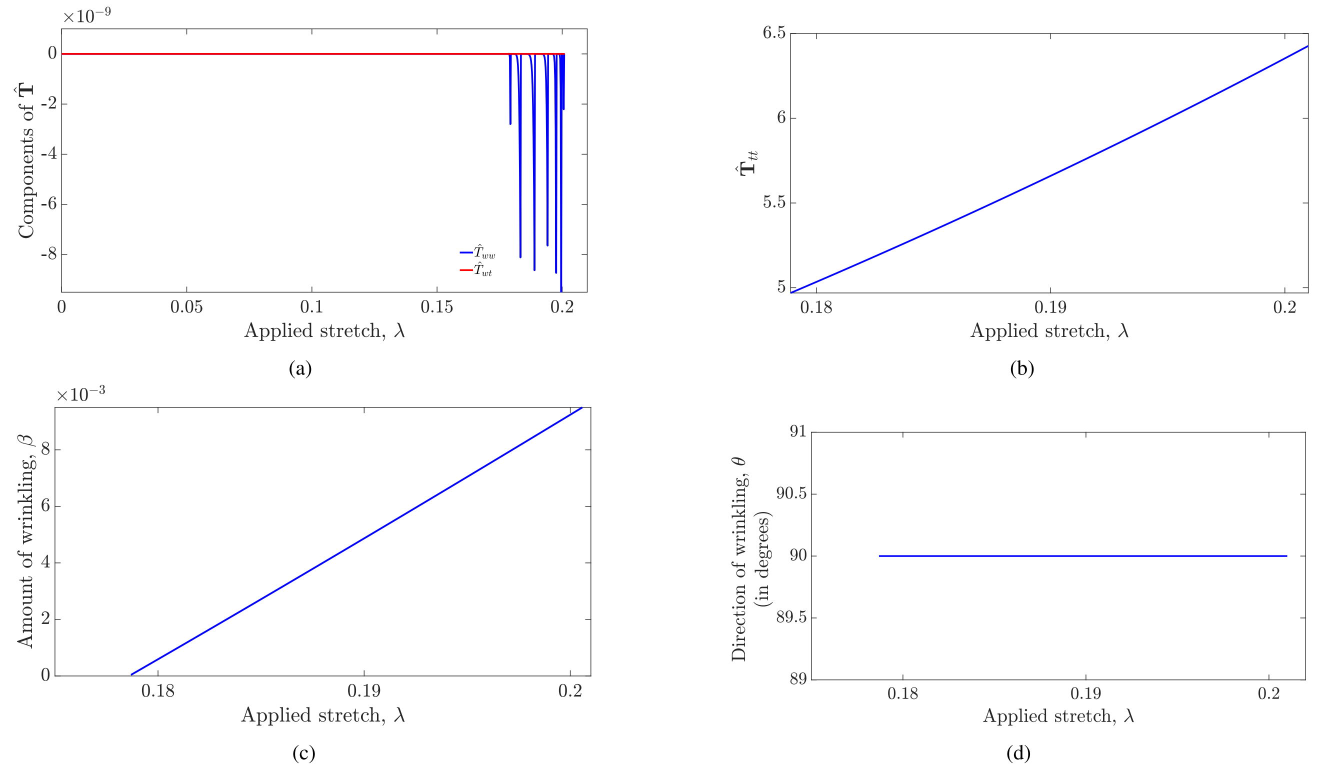

Fig. 6. Results of the numerical analysis of a wrinkled membrane under unequal-biaxial stretch for $\nu = 0.3$. Fig. (a) and (b) show the variation of different components of the Cauchy stress $\hat{\mathbf{T}}$ with the applied stretch λ. The variation of: (c) amount of wrinkling, β and, (d) its direction with the applied stretch $\lambda(t)$ are also shown.

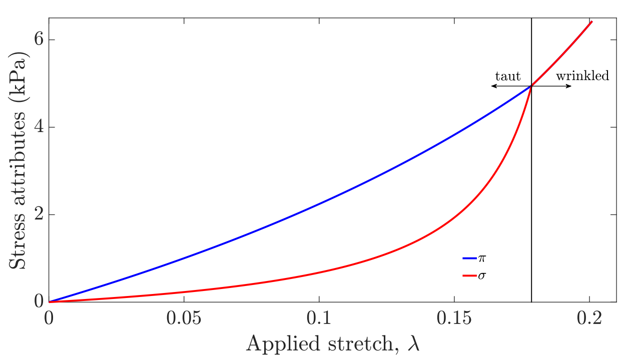

Fig. 7. Variations of the dilational stress π and the squeeze stress σ with the applied stretch $\lambda(t)$.

Results of the numerical analysis for this motion are shown in Fig. 8. The variations of the components $\hat{T}_{ww}$ and $\hat{T}_{wt}$ are shown in Fig. 8(a). The maximum error in this numerical analysis is found to be 9.68×10^{-9}. Moreover, as shown in Fig. 8(b), $\hat{T}_{tt}$ remains positive throughout the motion. Figs. 8(c) and 8(d) show the variation of the amount and direction of wrinkling with the applied stretch Λ. While the direction of wrinkles remain constant at $\theta \simeq 90°$, the magnitude of β increases with the applied stretch Λ, similar to the case of an unequal-biaxial stretch.

In case of a uniaxial stretch, the stress attributes follow a trend similar to that of a biaxial stretch, i.e., $\bar{\pi} = \bar{\sigma}$ and $\tau = 0$ throughout the deformation. This is due to the fact that in both cases, the matrix of the deformation gradient is a diagonal matrix and the direction of wrinkles $\theta \simeq 90°$. Fig. 9 shows the variation of the squeeze stress with and without the consideration of wrinkling. It is evident that the increase in squeeze stress is more gradual for a wrinkled membrane. The implication of this difference will be discussed in Section 5.1.

5. Discussions

5.1. Implications on the identification of material parameters

The idea of using a **QR** kinematics-based framework, as opposed to the traditional polar decomposition-based kinematics and invariants-based constitutive theories, originated from the need for a better method to interpret experimental data. As Criscione and co-workers (Criscione et al., 2000; Criscione, 2003) showed, although the traditional invariant theory is a mathematically sophisticated approach in constitutive modeling, the covariance between the invariants makes it difficult to parameterize the material models, especially for soft materials. A **QR** framework is of great help in that aspect because of the minimum covariance between different modes of deformation used in constitutive modeling. Due to this advantage, a **QR**-framework has been successfully employed in identifying material parameters for soft biological membranes (Kazerooni et al., 2019) and elastomers (Jiang et al., 2022). In this framework, three experiments are required to identify the complete set of material parameters for a biological membrane: an equibiaxial stretch for A_1 and B_1, a uniaxial stretch for A_2 and B_2 and a simple shear for A_3 and B_3. The experimental setup and protocols for the first two tests were developed by Jiang et al. (2021) whereas the test setup for the latter was developed by Sridhar et al. (2025). Despite being a promising approach in material parameter identification for biological membranes, this method currently suffers from a major shortcoming as revealed by the wrinkling analysis performed here. As shown in Section 4, for both uniaxial stretch and simple shear, a biological membrane wrinkles as soon as the motion begins. Moreover, the stress–strain relationships for the respective squeeze and shear modes of deformation differ significantly for a wrinkled membrane as compared to their taut counterpart as shown in Figs. 4(a) and 9. Therefore, identifying the material parameters by comparing experimental data with the constitutive relation (12) would be erroneous, since this model was derived under the assumption of a taut membrane. Instead, one

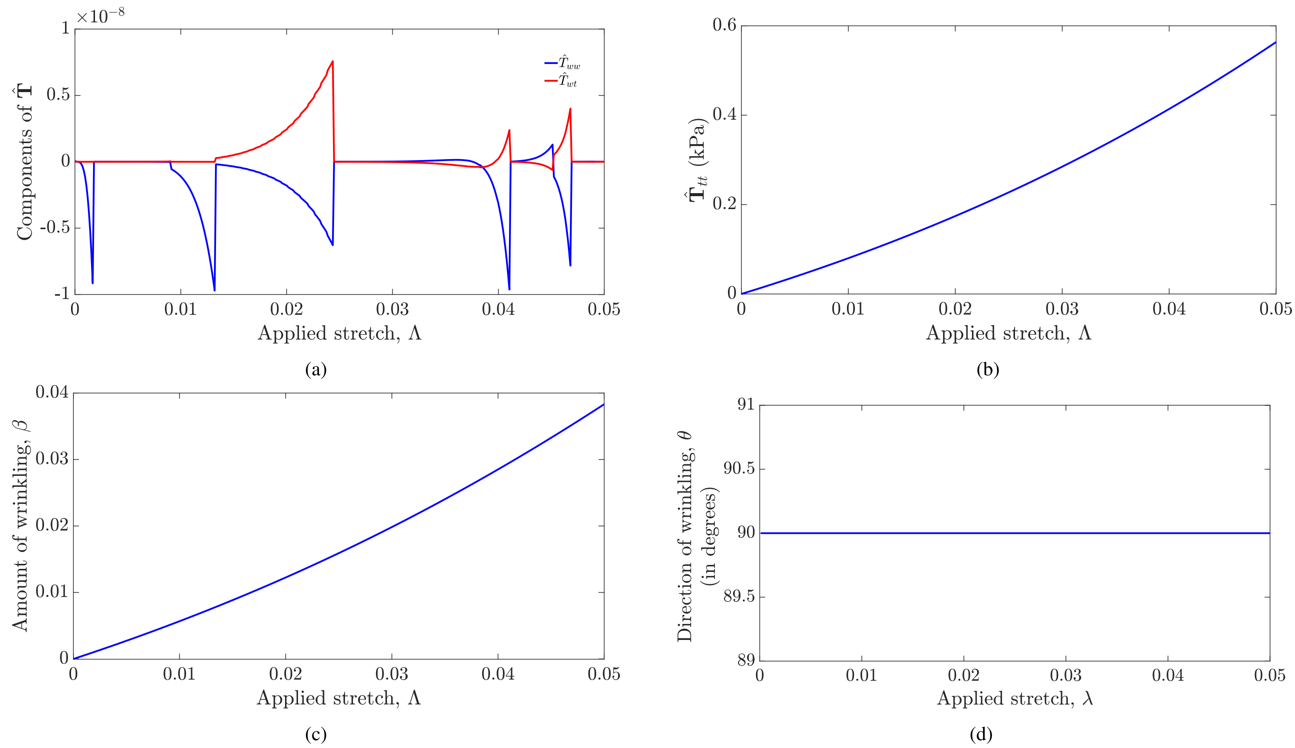

Fig. 8. Results of the wrinkle analysis for a uniaxial stretch. The figure shows a variation of: (a) $\hat{T}_{ww}$ and $\hat{T}_{wt}$ components of the rotated Cauchy stress that measure errors in the numerical analysis, (b) the component $\hat{T}_{tt}$, (c) amount of wrinkling, β and, (d) its direction with the applied stretch $\Lambda(t)$ for its entire admissible range.

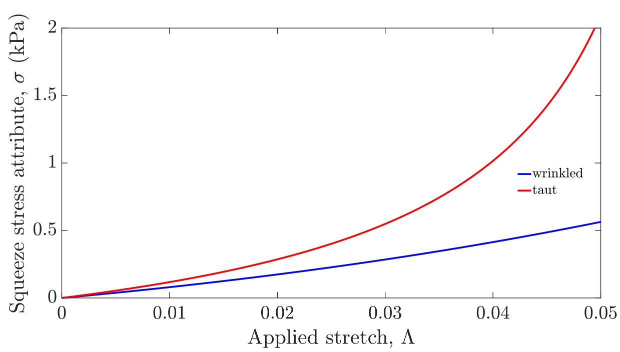

Fig. 9. Comparison of the squeeze stress attribute σ with and without taking wrinkling into consideration.

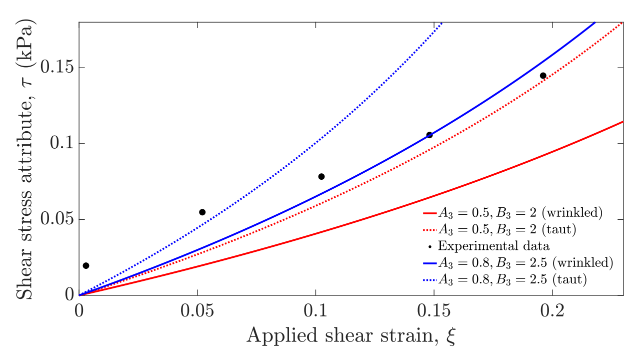

Fig. 10. A method to identify the material parameters A_3 and B_3. The solid and dotted lines show the shear stress response of the membrane with and without taking wrinkles into account, respectively. The initial material parameters $A_3 = 0.5, B_3 = 2$ are modified to $A_3 = 0.8, B_3 = 2.5$ such that the response of the wrinkled member fits with the experimental data of Dokos et al. (2002). (For interpretation of the references to color in this figure legend, the reader is referred to the web version of this article.)

needs to compare the stress–strain curve for a wrinkled membrane with the experimental data to characterize the parameters A_2, B_2 and A_3, B_3. Since the membrane remains in a taut state under an equibiaxial stretch, such a modification is not required for obtaining the material parameters A_1 and B_1, associated with dilation.

Having established the need to modify the material characterization procedure, we now demonstrate a method to identify the parameters A_3 and B_3 using the digitized experimental data of Dokos et al. (2002). Since the amount and direction of wrinkling are not known *a priori* and need to be calculated via the numerical method provided in Section 3.3, the material parameter identification essentially becomes an iterative process. Let us first assume that the membrane remains taut under the application of a simple shear. Needless to say that under this assumption, the material parameters are the same as the ones given in Table 2, i.e., $A_3 = 0.5, B_3 = 2$. The red lines in Fig. 10 show the stress–strain curves for these parameters with solid and dotted lines indicating the responses of the membrane with and without taking wrinkling into consideration. Because of the differences in the stress response due to wrinkling, the stress–strain curve for the wrinkled membrane (solid red line) does not fit well with the experimental data. Therefore, the material parameters are now optimized to $A_3 = 0.8, B_3 = 2.5$ such that the response of the wrinkled membrane (solid blue line) fits relatively better with the experimental data. It can easily be observed from Fig. 10 that the response of the taut membrane (dotted blue line) for the modified material parameters, i.e., $A_3 = 0.8, B_3 = 2.5$ differs significantly from the experimental data. Since the membrane wrinkles throughout the motion, $A_3 = 0.8, B_3 = 2.5$ are the corrected material parameters. More details on the procedure of a wrinkle-aware material parameter identification and a brief discussion on parameter identifiability are provided in Appendix.

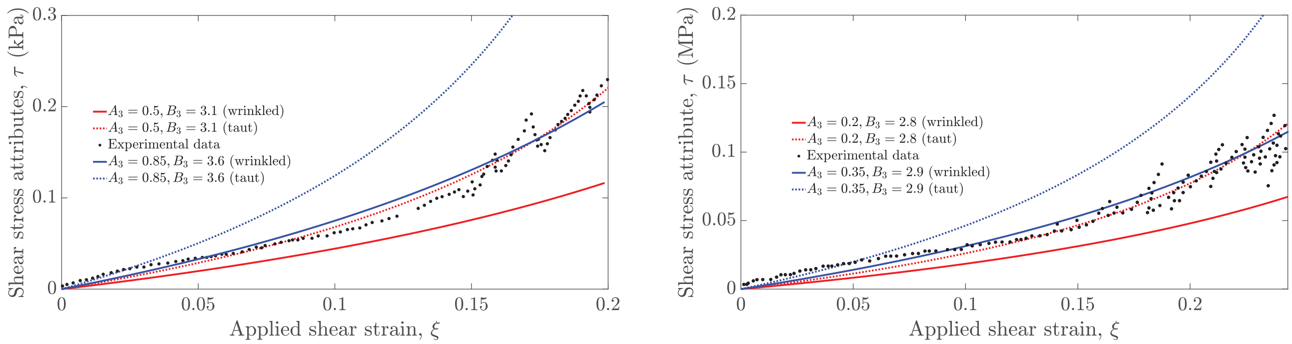

(a) (b)

Fig. 11. Identification of material parameters for a simple shear test on rat skin samples. The parameters were obtained by comparing the response of the wrinkled membrane with the experimental data of Sridhar et al. (2025) for two samples, cut along (a) the Cranial–Caudal and (b) the Medial–Lateral directions.

A similar procedure was followed to obtain the material parameters for a rat skin by comparing the response of a wrinkled membrane with the digitized experimental data of Sridhar et al. (2025). For this purpose, the stress–strain curves for a simple shear test on two rat skin samples, cut along the Cranial–Caudal and the Medial–Lateral directions have been used. It is worth noting that in the original paper, the off-diagonal terms of a Kirchhoff stress and a Green strain were used to plot the respective stress–strain curves. Since the matrix of a deformation gradient is upper-triangular and $\boldsymbol{\mathcal{R}} = \mathbf{I}$ for a simple shear, the off-diagonal term of the Kirchhoff stress is the same as the shear stress attribute, τ. Moreover, for a deformation gradient of the form (36), the off-diagonal term of the Green strain[4] also equals to the shear strain attribute, γ. Now following the same exercise as before, the material parameters for these two samples have been identified. As shown in Fig. 11(a), a simple fitting of the experimental data with the constitutive model (12) leads to an erroneous identification of the material parameters as $A_3 = 0.5$ and $B_3 = 3.1$. This error is rectified when the response of the wrinkled membrane is considered for comparison with the experimental data. Following the procedure delineated in Appendix, the corrected material parameter is obtained as $A_3 = 0.85$ and $B_3 = 3.6$. In a similar manner, the corrected material parameters for the rat skin cut along the Medial–Lateral direction is obtained as $A_3 = 0.35$ and $B_3 = 2.9$, as shown in Fig. 11(b). A similar exercise can be carried out for a uniaxial stretch.

5.2. Anisotropic membranes

As shown by Erel and Freed (2017), Freed (2017) and Paul (2025), the effect of anisotropy enters into the **QR** framework through an encoding/decoding map between the stress/strain attributes and the corresponding Kirchhoff stress $\boldsymbol{\mathcal{S}}$ and velocity gradient $\boldsymbol{\mathcal{L}}$. In terms of the components of the Laplace stretch, the dilational and squeeze strain attributes for an anisotropic membrane can be written as

$$\delta = \frac{1}{2}\ln\left(a^n\, b^{1/n}\right) \quad \text{and,} \quad \varepsilon = \frac{1}{2}\ln\left(a^{1/n}/b^n\right) \tag{48}$$

where $n > 0$ is a parameter representing the strength of anisotropy. The relationship between the stress attributes and the Kirchhoff stress using the encoding/decoding maps can be written as (Erel and Freed, 2017)

$$\begin{pmatrix}\pi\\ \sigma\\ \tau\end{pmatrix} = \begin{bmatrix}1/n & n & 0\\ 1/n & -n & 0\\ 0 & 0 & a/b\end{bmatrix}\begin{pmatrix}\mathcal{S}_{11}\\ \mathcal{S}_{22}\\ \mathcal{S}_{12}\end{pmatrix} \quad \text{and,}$$

$$\begin{pmatrix}\mathcal{S}_{11}\\ \mathcal{S}_{22}\\ \mathcal{S}_{12}\end{pmatrix} = \begin{bmatrix}n/2 & n/2 & 0\\ 1/2n & -1/2n & 0\\ 0 & 0 & b/a\end{bmatrix}\begin{pmatrix}\pi\\ \sigma\\ \tau\end{pmatrix}. \tag{49}$$

It is important to note that the strength of anisotropy enters into our constitutive model only through the encoding/decoding maps while the form of the internal energy, given in Eq. (11), remains unaltered. We shall now examine the effect of anisotropy on the wrinkling criteria and the subsequent numerical analysis.

From Eq. (22), it is evident that the criterion for slacking is determined based on the numerical values of the components of Laplace stretch a, b and γ which can be directly obtained from the matrix of the deformation gradient, $\tilde{\mathbf{F}}$ using a Gram–Schmidt procedure. Since the derived strain attributes δ and ε are not required for this criterion, the slacking criterion remains the same for an anisotropic membrane. On the other hand, the criterion for a taut membrane is derived from the invariants of the Kirchhoff stress $\boldsymbol{\mathcal{S}}$ which is related to the stress attributes through the decoding map $(49)_2$. Hence, the criterion for a taut membrane needs to be modified accordingly. The modified criterion for a taut, anisotropic membrane reads

$$\begin{aligned}&\operatorname{tr}(\boldsymbol{\mathcal{S}}) \geq 0 \implies n(\pi+\sigma) + \frac{1}{n}(\pi-\sigma) \geq 0 \implies \pi \geq \left(\frac{1-n^2}{1+n^2}\right)\sigma\\ &\det(\boldsymbol{\mathcal{S}}) \geq 0 \implies \pi^2 \geq \sigma^2 + 4b^2\,\tau^2/a^2.\end{aligned} \tag{50}$$

Therefore, in addition to the condition $(50)_2$, we have another criterion for a taut, anisotropic membrane that depends on the strength of anisotropy, n. Needless to say that the modified criterion for a taut membrane is the same as Eq. (21) when $n = 1$. Note that the condition (50) reduced to a single inequality, $\pi \geq \sqrt{\sigma^2 + 4b^2\tau^2/a^2}$ for an isotropic membrane using the fact that the dilation stress must be non-negative for a taut membrane. For an anisotropic membrane, such a reduction is not possible since the strength of anisotropy parameter, n can take values both greater and less than one. In particular, when $n > 1$, the direction -1 is stiffer than the direction -2 whereas $n < 1$ implies that the direction -2 is stiffer. Therefore, the former condition may allow for the dilational stress to be negative even when the membrane is taut.

For the numerical analysis of wrinkling in an anisotropic membrane, the method developed in Section 3.3 remains almost the same except for the definitions of strain and stress attributes. In view of the above discussion, Eqs. (31) and (33) in Section 3.3 need to be replaced with Eqs. (48) and (49), respectively. The rest of the numerical procedure remains the same.

6. Concluding remarks

In this paper, we studied the wrinkling behavior of a strain-limiting membrane derived from the theory of implicit elasticity. The constitutive model for the membrane was developed using a **QR** decomposition

[4] Unfortunately, a wrong definition of the Green strain, $\mathbf{E} = 1/2(\mathbf{F}\mathbf{F}^\top - \mathbf{I})$ was used by Sridhar et al. (2025). Nevertheless, the experimental data can still be used since the off-diagonal term in the computed strain is the same as our shear strain attribute, γ.

of the deformation gradient that enables a mode-wise characterization of the membrane response. Criteria for a taut, wrinkled and slacked membrane within the chosen framework have been derived. The response of the wrinkled membrane is determined using the method of Roddeman (1991) in which a fictitious deformation is imposed on the wrinkled membrane such that it is virtually stretched to a fictitious, taut state. Thereafter, the amount and direction of wrinkling are determined from the condition of a uniaxial, tensile state of the Cauchy stress, represented in a local coordinate system of the wrinkled membrane. In our framework, this procedure leads to a system of highly nonlinear, coupled, algebraic equations. A modified Broyden's method with a derivative-free line search algorithm has been used to solve this system of equations. Using this model, three homogeneous boundary value problems, viz., a simple shear, an unequal-biaxial and a uniaxial stretch (squeeze), have been studied. The boundary value problem involving an unequal-biaxial stretch shows a particularly interesting result as the criterion for wrinkling is met due to the difference in the maximum allowable strain for different modes of deformation. This is a direct consequence of the strain-limiting behavior exhibited by biological membranes. We conclude this paper with a discussion on the implication of wrinkling on the identification of material parameters and a method for wrinkling analysis in anisotropic, implicit elastic membranes. This work can be further extended to perform a full-scale finite element analysis of thin-walled biological membranes in the future.

Declaration of competing interest

The authors declare that they have no known competing financial interests or personal relationships that could have appeared to influence the work reported in this paper.

Appendix. Method for wrinkle-aware parameter identification and its potential limitations

In this section, we demonstrate a method for identification of material parameters from relevant experimental data taking wrinkling into account. Since the procedure of determining the required stress response for a wrinkled membrane is highly nonlinear and both the amount of wrinkling, β and its direction, $\mathbf{w}$ depend on the material parameters, identification of these parameters is slightly more convoluted than a direct curve fitting technique, commonly used for material characterization in nonlinear elasticity. At the outset, let us define the coefficient of determination, R^2 as

$$R^2 = 1 - \frac{\sum_{i=1}^{n}(\mathscr{S}_{\text{model}_i} - \mathscr{S}_{\text{experiment}_i})^2}{\sum_{i=1}^{n}(\mathscr{S}_{\text{experiment}_i} - \overline{\mathscr{S}}_{\text{experiment}})^2},$$
$$\overline{\mathscr{S}}_{\text{experiment}} = \frac{1}{n}\sum_{i=1}^{n}\mathscr{S}_{\text{experiment}_i} \quad \text{(A.1)}$$

where $\mathscr{S}_{\text{model}}$ represents the squeeze or shear stress attributes associated with the corresponding experimentally measured strain attributes, as obtained via the numerical method in Section 3.3 whereas $\mathscr{S}_{\text{experiment}}$ represents their corresponding experimental counterparts. The material parameters are then obtained by maximizing R^2 with respect to admissible values of the material parameters. The procedure for a wrinkle-aware material parameter identification is provided in Alg. 2. In this method, a simultaneous variation of both the material parameters is required to identify their optimum values due to the high nonlinearity associated with the determination of $\mathscr{S}_{\text{model}}$. With a slight abuse of notation, we drop the subscripts from these parameters in Alg. 2, i.e., A_α and $B_\alpha, \alpha = 2, 3$ are simply written as A and B. We denote the respective admissible range (parameter space) of A and B as $\mathscr{D}_A$ and $\mathscr{D}_B$. The rest of the procedure is described in Alg. 2.

Let us now discuss this procedure with the experimental data shown in Fig. 11. The heat maps of R^2 for variations in A_3 and B_3 are shown in Fig. A.12. For the sample cut along the Cranial–Caudal direction (Fig. A.12(a)), some combinations of A_3 and B_3 show negative R^2 values, indicating a very poor fit with the experimental data. These values have been removed from the R^2 matrix in order to produce a more meaningful heat map. As observed from Fig. A.12, the optimum values for A_3 and B_3 are $A_3 = 0.85, B_3 = 3.6$ producing $R^2 = 0.969$ for a sample cut along the Cranial–Caudal direction and, $A_3 = 0.35, B_3 = 2.9$ producing $R^2 = 0.939$ for a sample cut along the Medial–Lateral direction, respectively. Note that these optimum values of material parameters have been used in Fig. 11.

Algorithm 2 A method for a wrinkle-aware parameter identification

Require: Experimental data for a specific mode of deformation
Require: $\mathscr{D}_A$ and $\mathscr{D}_B$
  Discretize $\mathscr{D}_A$ and $\mathscr{D}_B$ into m and n equally spaced points
  for $i = 1$ to m **do**
    for $j = 1$ to n **do**
      Use $\tilde{A} \leftarrow \mathscr{D}_A(i)$ and $\tilde{B} \leftarrow \mathscr{D}_B(j)$
      Compute $\mathscr{S}_{\text{model}}$ following the steps in § 3.3 and using Alg. 1 with $\tilde{A}$ and $\tilde{B}$
      Compute $R^2(j, i)$ using Eq. (A.1)
    end for
  end for
  Compute $\max_{i,j} R^2$ and its location $\leftarrow (\bar{j}, \bar{i})$
  $A \leftarrow \mathscr{D}_A(\bar{i})$ and $B \leftarrow \mathscr{D}_B(\bar{j})$
  return A and B

From Fig. A.12, it can be further observed that the R^2 values mostly do not follow a particular pattern, especially for the data shown in Fig. A.12(a). Moreover, in some cases, the R^2 values are very close (e.g., $R^2 = 0.969$ for $A_3 = 0.85, B_3 = 3.6$ and, $R^2 = 0.9675$ for $A_3 = 0.8, B_3 = 3.8$ in Fig. A.12(a)) and hence, using either of these material parameter pairs would not significantly alter the model prediction. The lack of pattern in R^2 and potential non-uniqueness of the material parameters could be attributed to the high nonlinearity associated with the wrinkling analysis as well as the noise in the experimental data. This observation begs a question whether it is always possible to determine the optimum values of the material parameters uniquely, especially for a noisy experimental data set. To resolve this issue reliably, one has to study a larger experimental data set and possibly use sophisticated uncertainty quantification techniques. With these tools, the wrinkle-aware material parameter identification can be made more robust, however, this is beyond the scope of the current paper. As a proof-of-concept, we perform a rudimentary sensitivity analysis to understand the effects of experimental noise on the parameter identification procedure.

For this analysis, an experimental data set and the derived material parameters are considered to be inputs and outputs, respectively. The experimental data for rat skin sample cut along the Cranial–Caudal direction (Fig. 11(a)) have been used as a base data. Let us introduce an artificial noise to this experimental data set such that the data with additional noises becomes

$$\mathscr{S}_{\text{noise}_i} = \mathscr{S}_{\text{experiment}_i} + \varphi \times \max\{|\mathscr{S}_{\text{experiment}_i}|\} \times \mathcal{N}(0, 1) \quad \text{(A.2)}$$

where $\mathscr{S}_{\text{noise}}$ and $\mathscr{S}_{\text{experiment}}$ are the experimental data with and without additional noise, respectively; φ is the noise level and $\mathcal{N}(0, 1)$ is a random number drawn from a standard normal distribution. Here we use a noise level of 1%, 5%, 10% and 15% and, determine the optimum values for a material parameter keeping the other parameter fixed at the base value (i.e., optimum value at $\varphi = 0$) for different levels of noises using Alg. 2. For each noise level, ten realizations have been considered. The range of optimum material parameters for these realizations and the associated R^2 are presented in Table A.3. It can be observed that for a noise level of 1–10%, while the optimum values

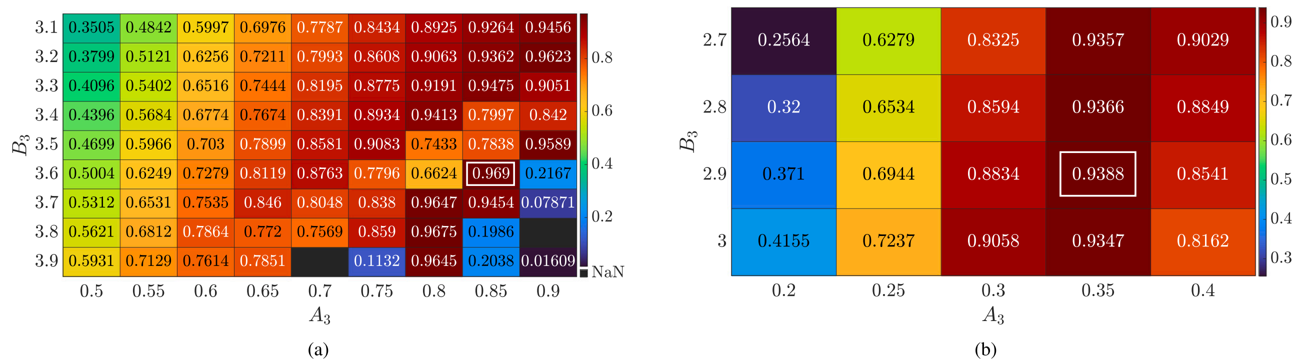

Fig. A.12. Heat maps of the coefficient of determination, R^2 with respect to material parameters A_3 and B_3 for the experimental data of Sridhar et al. (2025) for a sample of rat skin cut along *(a)* the Cranial–Caudal and *(b)* the Medial–Lateral directions. Each cell in the heat map shows the corresponding values of R^2. The maximum values for R^2 are highlighted with a white box around it.

Table A.3
Optimum values of material parameters with respect to the base values (A_3 = 0.9 and B_3 = 3.5) for varying noise levels, φ.

A_3, B_3 and R^2 \ φ	0.00	0.01	0.05	0.10	0.15
A_3 (for fixed $B_3 = 3.6$)	0.85	0.85	0.85	0.85	0.7–0.85
R^2 for optimum A_3	0.969	0.965–0.969	0.921–0.943	0.839–0.877	0.662–0.784
B_3 (for fixed $A_3 = 0.85$)	3.6	3.6	3.6	3.6	3.1–3.7
R^2 for optimum B_3	0.969	0.965–0.968	0.931–0.948	0.837–0.888	0.732–0.782

for the material parameters remain the same, their corresponding R^2-values decrease with increasing φ. However, for a noise level of 15%, both parameters vary significantly while their R^2-values are within the range of 0.66–0.78, indicating a relatively poor fit with the noisy experimental data. As a consequence, this analysis shows that the parameter identification procedure in Alg. 2 is indeed sensitive to high level of experimental noise and thus, there is a need for a more robust parameter identification algorithm that would address these issues. As stated earlier, development of such an algorithm, however, is beyond the scope of the current paper and remains an open problem for further investigation.

Data availability

Data will be made available on request.

References

Avazmohammadi, R., Li, D.S., Leahy, T., Shih, E., Soares, J.S., Gorman, J.H., Gorman, R.C., Sacks, M.S., 2018. An integrated inverse model-experimental approach to determine soft tissue three-dimensional constitutive parameters: application to post-infarcted myocardium. Biomech. Model. Mechanobiol. 17 (1), 31–53.

Bilby, B.A., Bullough, R., Smith, E., 1955. Continuous distributions of dislocations: a new application of the methods of non-Riemannian geometry. Proc. R. Soc. A 231 (1185), 263–273.

Broyden, C.G., 1965. A class of methods for solving nonlinear simultaneous equations. Math. Comp. 19 (92), 577–593.

Bulíček, M., Málek, J., Rajagopal, K.R., Walton, J.R., 2015. Existence of solutions for the anti-plane stress for a new class of strain-limiting elastic bodies. Calc. Var. Partial Differential Equations 54 (2), 2115–2147.

Bustamante, R., Rajagopal, K., 2015. Solutions of some boundary value problems for a new class of elastic bodies undergoing small strains. comparison with the predictions of the classical theory of linearized elasticity: Part i. problems with cylindrical symmetry. Acta Mech. 226 (6), 1815–1838.

Cermelli, P., Gurtin, M.E., 2001. On the characterization of geometrically necessary dislocations in finite plasticity. J. Mech. Phys. Solids 49 (7), 1539–1568.

Clayton, J., Freed, A., 2020. A constitutive framework for finite viscoelasticity and damage based on the Gram–Schmidt decomposition. Acta Mech. 231 (8), 3319–3362.

Clayton, J.D., Freed, A., 2020. A constitutive model for lung mechanics and injury applicable to static, dynamic, and shock loading. Mech. Soft Mater. 2 (1), 1–35.

Criscione, J.C., 2003. Rivlin's representation formula is ill-conceived for the determination of response functions via biaxial testing. J. Elasticity 70 (1), 129–147.

Criscione, J.C., Humphrey, J.D., Douglas, A.S., Hunter, W.C., 2000. An invariant basis for natural strain which yields orthogonal stress response terms in isotropic hyperelasticity. J. Mech. Phys. Solids 48 (12), 2445–2465.

Dokos, S., Smaill, B.H., Young, A.A., LeGrice, I.J., 2002. Shear properties of passive ventricular myocardium. Am. J. Physiol.-Heart Circ. Physiol. 283 (6), H2650–H2659.

Epstein, M., 1999. On the wrinkling of anisotropic elastic membranes. J. Elasticity 55 (2), 99–109.

Epstein, M., Forcinito, M.A., 2001. Anisotropic membrane wrinkling: theory and analysis. Int. J. Solids Struct. 38 (30–31), 5253–5272.

Erel, V., Freed, A.D., 2017. Stress/strain basis pairs for anisotropic materials. Composites B 120, 152–158.

Fehervary, H., Smoljkić, M., Vander Sloten, J., Famaey, N., 2016. Planar biaxial testing of soft biological tissue using rakes: A critical analysis of protocol and fitting process. J. Mech. Behav. Biomed. Mater. 61, 135–151.

Freed, A.D., 2017. A note on stress/strain conjugate pairs: explicit and implicit theories of thermoelasticity for anisotropic materials. Internat. J. Engrg. Sci. 120, 155–171.

Freed, A., Erel, V., Moreno, M., 2016. Conjugate stress/strain base pairs for planar analysis of biological tissues. J. Mech. Mater. Struct. 12 (2), 219–247.

Freed, A.D., Liao, J., Einstein, D.R., 2014. A membrane model from implicit elasticity theory: application to visceral pleura. Biomech. Model. Mechanobiol. 13 (4), 871–881.

Freed, A.D., Rajagopal, K., 2016a. A promising approach for modeling biological fibers. Acta Mech. 227 (6), 1609–1619.

Freed, A.D., Rajagopal, K., 2016b. A viscoelastic model for describing the response of biological fibers. Acta Mech. 227 (12), 3367–3380.

Fung, Y., 1967. Elasticity of soft tissues in simple elongation. Am. J. Physiol.-Leg. Content 213 (6), 1532–1544.

Fung, Y.-c., 2013. Biomechanics: Mechanical Properties of Living Tissues. Springer Science & Business Media.

Hakimzadeh, M., Agrawal, V., Dayal, K., Mora-Corral, C., 2022. Phase-field finite deformation fracture with an effective energy for regularized crack face contact. J. Mech. Phys. Solids 167, 104994.

Hakimzadeh, M., Walkington, N., Mora-Corral, C., Gazonas, G., Dayal, K., 2025. Crack face contact modeling is essential to predict crack-parallel stresses. J. Appl. Mech. 92, 9.

Jarasjarungkiat, A., Wüchner, R., Bletzinger, K.-U., 2008. A wrinkling model based on material modification for isotropic and orthotropic membranes. Comput. Methods Appl. Mech. Engrg. 197 (6–8), 773–788.

Jenkins, C., Leonard, J., 1993. Dynamic wrinkling of viscoelastic membranes. J. Appl. Mech. 60 (3), 575–582.

Jiang, M., Sridhar, R.L., Robbins, A.B., Freed, A.D., Moreno, M.R., 2021. A versatile biaxial testing platform for soft tissues. J. Mech. Behav. Biomed. Mater. 114, 104144.

Jiang, M., Wang, Z., Freed, A.D., Moreno, M.R., Erel, V., Dubrowski, A., 2022. Extracting material parameters of silicone elastomers under biaxial tensile tests using virtual fields method and investigating the effect of missing deformation data close to specimen edges on parameter identification. Mech. Adv. Mater. Struct. 29 (27), 6421–6435.

Kachanov, M., 1980. Continuum model of medium with cracks. J. Eng. Mech. Div. 106 (5), 1039–1051.

Kang, S., Im, S., 1997. Finite element analysis of wrinkling membranes. J. Appl. Mech. 64, 263–269.

Kazerooni, N.A., Srinivasa, A., Freed, A., 2019. Orthotropic-equivalent strain measures and their application to the elastic response of porcine skin. Mech. Res. Commun. 101, 103404.

Kohn, R.V., O'Brien, E., 2018. The wrinkling of a twisted ribbon. J. Nonlinear Sci. 28 (4), 1221–1249.

Li, D.-H., Fukushima, M., 2000. A derivative-free line search and global convergence of broyden-like method for nonlinear equations. Optim. Methods Softw. 13 (3), 181–201.

Li, X., Steigmann, D., 1995. Finite deformation of a pressurized toroidal membrane. Int. J. Non-Linear Mech. 30 (4), 583–595.

Lu, K., Accorsi, M., Leonard, J., 2001. Finite element analysis of membrane wrinkling. Internat. J. Numer. Methods Engrg. 50 (5), 1017–1038.

Lubarda, V., 2010. Constitutive analysis of thin biological membranes with application to radial stretching of a hollow circular membrane. J. Mech. Phys. Solids 58 (6), 860–873.

Massabò, R., Gambarotta, L., 2007. Wrinkling of plane isotropic biological membranes. J. Appl. Mech. 74 (3), 550–559.

Miyazaki, Y., 2006. Wrinkle/slack model and finite element dynamics of membrane. Internat. J. Numer. Methods Engrg. 66 (7), 1179–1209.

Morgan, A., 1966. Some properties of media defined by constitutive equations in implicit form. Internat. J. Engrg. Sci. 4 (2), 155–178.

Ortiz-Bernardin, A., Bustamante, R., Rajagopal, K., 2014. A numerical study of elastic bodies that are described by constitutive equations that exhibit limited strains. Int. J. Solids Struct. 51 (3–4), 875–885.

Patil, A., Nordmark, A., Eriksson, A., 2015. Wrinkling of cylindrical membranes with non-uniform thickness. Eur. J. Mech. A Solids 54, 1–10.

Paudel, S., Paul, S., 2023. A note on the derivation of quotient rules and their use in **QR** kinematics. Acta Mech. 234 (11), 5937–5946.

Paul, S., 2025. Incorporation of internal state variables and plastically-induced anisotropy into a constitutive model involving scalar, conjugate, stress/strain base pairs. Eur. J. Mech. A Solids 109, 105435.

Paul, S., Freed, A.D., 2020. Characterizing geometrically necessary dislocations using an elastic–plastic decomposition of Laplace stretch. Z. Angew. Math. Phys. 71 (6), 196.

Paul, S., Freed, A.D., 2021. A constitutive model for elastic–plastic materials using scalar conjugate stress/strain base pairs. J. Mech. Phys. Solids 155, 104535.

Paul, S., Freed, A.D., Benjamin, C.C., 2021. Application of the Gram–Schmidt factorization of the deformation gradient to a cone and plate rheometer. Phys. Fluids 33 (1), 017113.

Peek, R., 2000. Axisymmetric wrinkling of cylinders with finite strain. J. Eng. Mech. 126 (5), 455–461.

Pipkin, A., 1986. Continuously distributed wrinkles in fabrics. Arch. Ration. Mech. Anal. 95 (2), 93–115.

Pipkin, A.C., 1986. The relaxed energy density for isotropic elastic membranes. IMA J. Appl. Math. 36 (1), 85–99.

Pipkin, A.C., 1994. Relaxed energy densities for large deformations of membranes. IMA J. Appl. Math. 52 (3), 297–308.

Rajagopal, K.R., 2003. On implicit constitutive theories. Appl. Math. 48 (4), 279–319.

Rajagopal, K., 2014. On the nonlinear elastic response of bodies in the small strain range. Acta Mech. 225 (6), 1545–1553.

Rajagopal, K., Srinivasa, A., 2016. An implicit three-dimensional model for describing the inelastic response of solids undergoing finite deformation. Z. Angew. Math. Phys. 67 (4), 86.

Roddeman, D.G., 1991. Finite-element analysis of wrinkling membranes. Commun. Appl. Numer. Methods 7 (4), 299–307.

Rossi, R., Lazzari, M., Vitaliani, R., Oñate, E., 2005. Simulation of light-weight membrane structures by wrinkling model. Internat. J. Numer. Methods Engrg. 62 (15), 2127–2153.

Roychowdhury, S., DasGupta, A., 2015. Inflating a flat toroidal membrane. Int. J. Solids Struct. 67, 182–191.

Sacks, M.S., Sun, W., 2003. Multiaxial mechanical behavior of biological materials. Annu. Rev. Biomed. Eng. 5 (1), 251–284.

Shivam, Paul, S., 2026. A novel large-strain kinematic framework for fiber-reinforced laminated composites and its application in the characterization of damage. Internat. J. Engrg. Sci. 224, 104518.

Shmoylova, E., Dorfmann, A., 2009. Wrinkling of a fiber-reinforced membrane. J. Appl. Mech. 76 (1), 011011.

Sridhar, R., Jiang, M., Freed, A., Jastram, A., Robbins, A., Moreno, M., 2025. Double 4-bar shear: A novel apparatus and method for simple shear mechanical analysis of membranes. J. Mech. Behav. Biomed. Mater. 107113.

Srinivasa, A., 2012. On the use of the upper triangular (or QR) decomposition for developing constitutive equations for green-elastic materials. Internat. J. Engrg. Sci. 60, 1–12.

Srinivasa, A., 2015. On a class of gibbs potential-based nonlinear elastic models with small strains. Acta Mech. 226 (2), 571–583.

Steigmann, D.J., 1990. Tension-field theory. Proc. R. Soc. A 429 (1876), 141–173.

Steigmann, D., Pipkin, A., 1989a. Finite deformations of wrinkled membranes. Quart. J. Mech. Appl. Math. 42 (3), 427–440.

Steigmann, D., Pipkin, A., 1989b. Wrinkling of pressurized membranes. Trans. ASME 56, 624–628.

Tong, P., Fung, Y.-C., 1976. The stress–strain relationship for the skin. J. Biomech. 9 (10), 649–657.

Valanis, K., Panoskaltsis, V., 2005. Material metric, connectivity and dislocations in continua. Acta Mech. 175 (1), 77–103.

Weinberg, K., Neff, P., 2008. A geometrically exact thin membrane model—investigation of large deformations and wrinkling. Internat. J. Numer. Methods Engrg. 74 (6), 871–893.

Zamani, S., Paul, S., Kotiya, A.A., Criscione, J.C., Freed, A.D., 2021. Application of qr framework in modeling the constitutive behavior of porcine coronary sinus tissue. Mech. Soft Mater. 3 (1), 1–20.

Zhang, W., Zakerzadeh, R., Zhang, W., Sacks, M.S., 2019. A material modeling approach for the effective response of planar soft tissues for efficient computational simulations. J. Mech. Behav. Biomed. Mater. 89, 168–198.

Zhou, W., Zhang, L., 2020. A modified Broyden-like quasi-Newton method for nonlinear equations. J. Comput. Appl. Math. 372, 112744.